Pigment Cell & Melanoma Research

WILEY

ORIGINAL ARTICLE OPEN ACCESS

Dominant Negative Mitf Allele Impacts Melanophore and Xanthophore Development and Reveals Collaborative Interactions With Tfec in Zebrafish Chromatophore Lineages

Katia G. Korzeniwsky[1] | Pietro L.H. de Mello[1] | Yipeng Liang[1] | McKenna Feltes[2] | Steven A. Farber[2] | David M. Parichy[1,3]

[1]Department of Biology, University of Virginia, Virginia, USA | [2]Department of Biology, Johns Hopkins University, Baltimore, Maryland, USA | [3]Department of Cell Biology, University of Virginia, Virginia, USA

Correspondence: David M. Parichy (dparichy@virginia.edu)

Received: 30 December 2024 | **Revised:** 28 February 2025 | **Accepted:** 8 March 2025

Funding: This work was supported by the National Institute of Diabetes and Digestive and Kidney Diseases and the National Institute of General Medical Sciences.

Keywords: genetic compensation | iridophore | melanophore | Mitf | Tfec | xanthophore | zebrafish

ABSTRACT

Ectothermic vertebrates exhibit a diverse array of pigment cell types—chromatophores—that provide valuable opportunities to uncover mechanisms of fate specification and how they evolve. Like melanocytes of mammals, the melanophores of teleosts and other ectotherms depend on basic helix–loop–helix leucine zipper transcription factors encoded by orthologues of *MITF*. A different chromatophore, the iridescent iridophore, depends on the closely related transcription factor Tfec. Requirements for the specification of other chromatophore lineages remain largely uncertain. Here we identify a new allele of the zebrafish Mitf gene, *mitfa*, that results in a complete absence of not only melanophores but also yellow-orange xanthophores. Harboring a missense substitution in the DNA-binding domain identical to previously isolated alleles of mouse, we show that this new allele has defects in chromatophore precursor survival and xanthophore differentiation that extend beyond those of *mitfa* loss-of-function. Additional genetic analyses revealed interactions between Mitfa and Tfec as a likely basis for the observed phenotypes. Our findings point to collaborative roles for Mitfa and Tfec in promoting chromatophore development, particularly in xanthophore lineages, and provide new insights into evolutionary aspects of MITF functions across vertebrates.

1 | Introduction

The neural crest lineage is a classic system for understanding mechanisms of fate specification (Kelsh et al. 2021; Le Douarin 1999). In mammals and birds, subsets of neural crest-derived cells develop as melanocytes that can transfer melanin to keratinocytes for incorporation into hair or feathers (Brombin and Patton 2024; Tadokoro and Takahashi 2017). In other vertebrates, neural crest cells, or latent progenitors derived from them, differentiate into several types of pigment cells, or "chromatophores" that retain their pigments intracellularly (Irion et al. 2016; Parichy 2021; Schartl et al. 2016). These include black melanophores, containing melanin; yellow or orange xanthophores; as well as red erythrophores that contain pteridines, carotenoids, or both; iridescent iridophores with crystalline guanine reflecting platelets; and white leucophores with deposits of guanine, uric acid, or other materials. Along with such a diverse array of readily visualized cell fates come outstanding opportunities to dissect mechanisms of specification and their evolution.

An essential specifier of melanocyte fate is *Microphthalmia Associated Transcription Factor* (*MITF*), allelic with the

Summary

- This work reveals new roles for MITF transcription factors in pigment cell development by identifying a dominant negative mutation in zebrafish Mitfa that eliminates both black melanophores and yellow xanthophores, unlike previously known loss-of-function mutations that affect only melanophores.
- Genetic analyses suggest collaborative functions of Mitfa and the related factor Tfec in promoting the development of both cell types.
- These findings provide new insights into the roles of MITF in pigment cell fate specification and evolutionary changes in MITF requirements across vertebrate lineages.

microphthalmia locus of mouse and a causal locus for Waardenburg syndrome type 2A and other disorders in humans (Hodgkinson et al. 1993; Tassabehji et al. 1994) *MITF* encodes a basic helix–loop–helix leucine zipper (bHLH-ZIP) transcription factor of the MiT subfamily positioned between key factors in neural crest development and downstream effectors of melanocyte fate: *MITF* expression depends on *SOX10*, *PAX3*, *LEF1*, and MITF; in turn, transactivates *TYRP1*, *DCT*, *MLENA*, and other genes required for melanization (reviewed in Goding and Arnheiter 2019; Vu et al. 2021). MITF also functions beyond differentiation, with critical roles in cell survival, regulating proliferation and invasion, lysosome biogenesis, autophagy, and other processes. The activity of MITF depends on phosphorylations downstream of receptor tyrosine kinases, most notably KIT, but roles for other post-translational modifications have been identified. MITF function also depends on interactions with co-factors including β-catenin and chromatin remodeling enzymes. Though MITF forms homodimers to bind M-box and a subset of E-box motifs at target loci, heterodimers with other MiT subfamily members TFEB, TFE3, and TFEC also bind DNA in vitro (Hemesath et al. 1994; Pogenberg et al. 2012).

In ectothermic vertebrates, orthologues of MITF are required for the specification and subsequent development of melanophores (Lister et al. 1999; Miyadai et al. 2023), whereas the MiT subfamily member Tfec has been implicated in the specification and differentiation of iridophores (Petratou et al. 2021). It remains uncertain whether other chromatophore lineages depend on "master regulators," like MITF in melanocytes of endotherms and melanophores of ectotherms, or how MITF or other MiT subfamily genes might be involved. Here, we report on a new semi-dominant mutant of zebrafish, *varo*, which has defects in melanophores and xanthophores when heterozygous and a complete absence of these cells when homozygous. We show that *varo* is allelic to the zebrafish Mitf gene *mitfa* and has a lesion in the basic region of the DNA binding domain identical to that of two alleles of mouse MITF that confer dominant negative activity. We find that *varo* mutants have defects in the survival of pigment cell progenitors and in the differentiation of xanthophores, with genetic analyses pointing to interactions between Mitf and Tfec in the development of chromatophore progenitors as well as xanthophores and iridophores. Our findings, along with other recent studies, suggest ancestral functions of MITF genes in melanophore and xanthophore development and a partitioning of such requirements among MiT family members in teleosts.

2 | Materials and Methods

2.1 | Zebrafish Stocks and Husbandry

Fish were reared at ~28°C (14 L:10D) with staging after (Kimmel et al. 1995) and (Parichy et al. 2009); juvenile fish were 11–16 mm standardized standard length (SSL) and young adult fish 20–26 mm SSL. All examples shown represent typical phenotypes observed for multiple individuals from multiple independent families, except where materials were limited for technical reasons, as in time-lapse image analyses, or biological reasons, as for semi-viability of *tfec* mutants, in which cases specific sample sizes are indicated. Fish were fed marine rotifers supplemented with Artemac (Reed Mariculture) as well as brine shrimp and GEMMA Micro (Skretting). All procedures were approved by the Animal Care and Use Committee of the University of Virginia (Protocol #4170) or the Carnegie Institution Department of Embryology Animal Care and Use Committee (Protocol #139). Fish lines were: *mitfa*^{c876} (*mitfa*^{varo}), *mitfb*, *tfec* (this study); *mitfa*^{w2} (Lister et al. 1999); *mitfa*^{vc7} (Johnson et al. 2011); *Tg(aox5:PALM-EGFP)*^{wprt12Tg}, *Tg(tyrp1b:PALM-mCherry)*^{wprt11Tg} (McMenamin et al. 2014); *Tg(NBT-dsRED)*^{zf148Tg} (Peri and Nusslein-Volhard 2008); *Tg(sox10:Eos)*^{w9Tg} (Prendergast et al. 2012); *Tg(mitfa:Eos)* (generously provided by J. Lister). Crosses were performed by natural spawning or in vitro fertilization after brief anesthesia using pharmaceutical grade MS222 (Syndel). Euthanasia was by overdose of MS222 followed by physical maceration.

2.2 | Still and Time-Lapse Imaging

Microscopic still images were collected on Zeiss AxioZoom and AxioObserver microscopes equipped with epifluorescence and Zeiss Axiocam cameras using ZEN Blue software, as well as a Zeiss LSM 880 microscope equipped with Fast Airyscan and ZEN Black software. Whole-fish images were collected with a Nikon digital SLR camera and a 105 mm MicroNikkor macro lens. For display, images were adjusted for levels, contrast, or color balance using Adobe Photoshop CS, with images of the same sets (e.g., fluorophores across genotypes) adjusted identically. In some microscopic images of fish older than 5 dpf, anesthetized individuals were treated briefly with 1 mg/mL epinephrine (Sigma-Aldrich) to contract pigment granules towards cell centers and enable visualization of pale yellow-orange carotenoid pigments of adult xanthophores. To further aid visualization, some figures of yellow-orange pigment deposits (in the absence of melanophores) were pseudocolored by converting bright field images to greyscale in Adobe Photoshop (color conversion settings: blue, 100, yellow, −75, all other, 0), inverting brightness values, and placing them under a Color Burn layer filled with color Hex Code #404040, thereby providing orange-yellow pigmentation on a dark background. Backgrounds in whole fish images shown in Figure S6a were removed digitally using Adobe Photoshop. Melanophores and xanthophores of wild-type and *varo*/+ siblings were counted in size-matched young adult fish in a region defined anteriorly and posteriorly

by the insertions of the anal fin, dorsally by the horizontal myoseptum, and ventrally by the ventral edges of the myotomes (Parichy et al. 2009).

Time-lapse images were collected using a Yokogawa CSU-X1M5000 laser spinning disk and a Hamamatsu camera mounted on a Zeiss AxioObserver microscope. Embryos were embedded in low-melting point agarose and imaged for 20 h, beginning at 22 h post-fertilization (22 hpf) with 10–15 min intervals between frames, depending on how many embryos were being imaged simultaneously.

For time-lapse imaging, numbers of cells and numbers of dying cells, defined by cellular fragmentation evident in ≥3 successive frames, were compared between genotypes with JMP Pro 18.0.1 for Apple Macintosh (JMP Statistical Discovery; jmp.com) using non-parametric statistics owing to heteroscedasticity of residuals and to avoid assumptions of underlying distributions. Numbers of cells in adults were compared by one-way analyses of variance.

2.3 | Forward Genetic Screening and Association Mapping by Pool Sequencing

Adult male AB* were mutagenized with N-ethyl-N-nitrosourea using standard methods (Solnica-Krezel et al. 1994) and were used to produce F1 offspring amongst which the *varo* mutant was identified for its semi-dominant phenotype. After isolating the mutant in the AB* background, we generated an F1 mapping cross using the wild-type WIK background and in-crossed two phenotypically mutant, heterozygous individuals to generate progeny segregating distinct wild-type, heterozygous, and homozygous mutant phenotypes in a ~1:2:1 proportion. We selected 100 wild-type and 100 homozygous mutant individuals to generate separate pools of genomic DNA sequenced with paired-end 150 bp (PE150) reads using a Hi-Seq X sequencer to a minimum of 20x coverage by Novogene. We employed a standard pipeline based on short-read next-generation sequencing (NGS) to call variants. Briefly, we filtered raw reads for quality and adapter sequences using *fastp* (Chen et al. 2018) with default parameters. We then aligned the cleaned reads to the reference zebrafish genome (GRCz11) with *bowtie2* (Langmead and Salzberg 2012) with default parameters. Following quality control with *Qualimap* (Okonechnikov et al. 2016), we removed low-quality reads and duplicates using *samtools* (Danecek et al. 2021) following the *GATK* best practice guidelines. We performed variant calling with *bcftools* (Li 2011), implementing custom filters to retain high-confidence variants with sufficient depth of coverage in both pools (MAPQ > 30, pool depth > 4, variant quality > 30, no missing data).

To identify *varo*, we sought regions of higher homozygosity, lower nucleotide diversity, and stronger population differentiation between the two pools and so calculated pool-sequence corrected measures of F_{st}, d_{xy}, and π using grenedalf (Czech et al. 2024). We also employed Fisher's Exact Test to identify regions with significant allele frequency differences between the pools. To narrow the candidate region, we combined the pipeline of (Bowen et al. 2012) with the haplotype-based approach of (Henke et al. 2017) and adapted the 'mapping score' statistic proposed by Bowen et al. (2012). We normalized the mapping score by weighing it with the total number of SNPs in each window squared and multiplying it by 100, resulting in a score between 0 and 100. A region with a high mapping score, therefore: (i) is highly homogeneous; and (ii) has a low number of loci from the mapping strain. This approach allowed us to pinpoint a specific region on chromosome 6 as the likely location of *varo*.

To identify potential causal variants, we obtained variant call sets (VCFs) from: (i) publicly available variants through NCBI and the National Human Genome Research Institute (NHGRI) (https://research.nhgri.nih.gov/manuscripts/Burgess/zebrafish/download.shtml), (ii) variants uploaded to Ensembl with *BioMart* (dataset: Zebrafish Short Variants) and (iii) a curated list of variants identified within our own lab. We concatenated, aligned, and filtered variants from all sequenced wild-type pools. Under the assumption that the *varo* phenotype arose from a novel variant induced by the ENU screen, we removed loci from the pooled sequencing dataset that: (i) were homozygous or heterozygous for a reference allele in the *varo*−/− pool; (ii) were homozygous or heterozygous for a variant previously identified in the NCBI, ENSEMBL, or in-house datasets; or (iii) were outside genic regions, according to the latest annotation of the GRCZ11 genome. We then used Ensembl's Variant Effect Predictor (*VEP*) (McLaren et al. 2016) to identify affected genes and transcripts, relative positions, and predicted functional consequences, and *SIFT* (Sorting Intolerant from Tolerant) (Sim et al. 2012) to assess the potential for deleterious effects. Data manipulation and visualization were facilitated by awk and *R* (v.4.3) (Team 2021) using the 'ggplot2,' 'ggrepel,' and 'tidyverse' packages.

2.4 | CRISPR/Cas9 Mutagenesis, Genotyping, and Reverse Transcriptase PCR

CRISPR/Cas9 mutants were generated by injecting one-cell stage embryos with ~1 nL of 5 μM gRNA:Cas9 RNP complex (IDT) (Hoshijima et al. 2019) and alleles recovered by incrossing and outcrossing. AltR sequences were (5′–3′): *mitfa*, AltR262 TAAGAGTCAAACTTGCCACA (exon 5a, upstream of DNA binding domain), AltR451 AGTAACCCATCGTCTCAAAG (−235–254 upstream of initiator codon), AltR465 CAAGGGTGGAGGACATGTCT (343 bp downstream of *mitfa* coding sequence); *mitfb*, AltR471 TTACTGATGGAGATTCCTGG (exon 4 upstream of DNA binding domain); *tfec*, AltR466 TCGTCAATAACTTCATCCAT (exon 3 targeting transcriptional activation domain, upstream of DNA binding domain) (Lister et al. 2011). For generating a *mitfa* allele that does not produce a transcript we co-injected AltR451 and AltR465, flanking conserved promoter elements and the gene body, and then selected for incrossing fish that lacked all melanophores and also lacked mitfa transcript by reverse transcriptase PCR. For testing *mitfa* transcript presence, total RNAs were isolated from 24 h post-fertilization embryos with Trizol, and oligo-dT primed cDNAs were prepared with SuperScript III (Thermo). Subsequent analyses of RNA-less fish revealed the loss of genomic PCR targets extending from upstream of the 5′ AltR into the first intron (~1 kb total) rather than through the 3′ AltR, a region apparently sufficient to prevent transcription, and suggesting the possibility of homology

directed repair to a larger initial deletion. Primers (forward, reverse; 5′–3′) for genotyping by Sanger sequencing or restriction digest were: *mitfa*^{w2}, mitfa-w2*_g261f,r (0 > Dra-I) ACAAGATGACACCAAATAACTACTGT,TTGCTGAAACTGGAATCTGAGAAA; *mitfa*^{varo} and *mitfa*^{vp70rc1varo}, mitfa_AltR262varo*_g695f,r TTTAAATGTCCAAGCTCACCATGC, TTAAACCGCCTTCTTCGTTCAACT; *mitfb*, mitfb_AltR471-g301f,r ATGCACATCAAATGACCGATTTCT, AGAATTCCCTTTTAACGCTGGTCA; *tfec*, tfec-ex3AltR-g332f,r ATGATGACGCGTCTGTTATTGGAT, TAATGCCACAGCACATACAACAGG. Primers for amplification of cDNAs were: *actb2*, actb2-c236f,r ATTGGCAATGAGAGGTTCAGGT, ACAATACAGTGTTGGCATACAGGT; *mitfa* full length, mitfa-M_FL-c1236f,r ATGTTGGAGATGCTCGAGTACAGTCACT, CTAACAGCCATTGTCATGTTCGTCCATAC; *mitfa* coding exons 2–4, mitfa-c300f,r CCCTCAACTGTGAGAAAGAGATGG, AAGAGTCAAACTTGCCACATGGTC. Primer sets for testing the region of genomic deletion (and outcomes) from 5′ to 3′ were: mitfa_del-g280f,r (deleted) TTATGCAGGATGAGTGGAACTAAA, ATTTAGGTGATGTGCAAGAACTGA; mitfa_del-g494f,r (deleted) AATCTTCTGTATGTTTGCATGCTT, TTTAGCTATTTTAAGGCAATGACA; mitfa_del-g246f,r (reduced size) ATCTCTGTTTGTGATTCAGGTTCA, TGTACCTCTTTCTCACAGTTGAGG; mitfa_del-g395f,r (retained) AACTGGCAAATGATAAATGTTGAA, TGAAAGGAAAAACATTTCATAATGC.

2.5 | Single Cell Transcriptomic Data

Analyses of published single-cell RNA-sequencing data used publicly available datasets (Aman et al. 2023; Saunders et al. 2019) with summations of transcript counts in Monocle3 (Cao et al. 2019) and 'tidyverse' and 'ggplot2' packages of *R*. Additional analyses were from datasets and analysis tools publicly accessible by web browsers (Sur et al. 2023), with output reformatted for presentation.

3 | Results

3.1 | Defects in Melanophore and Xanthophore Development in Embryonic and Adult *varo* Mutant Zebrafish

We recovered a semi-dominant adult pigment pattern mutant, *c876*, in a forward genetic screen for ENU-induced mutations. In keeping with our convention of naming dominant and semi-dominant pigment pattern mutants after surrealist painters, we designated the allele *varo* (Nonaka 2012).

Larvae heterozygous for *varo* exhibited irregular patterns, with melanophores having reduced amounts of melanin and sometimes occurring in ectopic locations (Figure 1a). Adults had body stripes with irregular borders and variable spacing between melanophores. Both melanophores and xanthophores had mild deficiencies in pigmentation as compared to the wild type, though the numbers of these cells were not significantly different between these genotypes (Figure 1b, upper; Figure S1a,b). In fins, melanophores, xanthophores, orange and white xantholeucophores (Lewis et al. 2019), and small numbers of iridophores were present, as in the wild type, yet white melanoleucophores (Huang et al. 2025) of the dorsal and caudal fin tips were almost completely absent (Figure 1b, lower; Figure S1d).

Fish homozygous for *varo* had far more severe phenotypes. Early larvae were devoid of melanophores and xanthophores, though iridophores were present in their typical locations (e.g., dorsal midline; Figure 1a). Similarly, in adults, melanophores and xanthophores were absent from the body, whereas iridophores were retained in a pattern similar to that of other mutants lacking melanophores or both melanophores and xanthophores, as in fish homozygous for presumptive null alleles of *mitfa* or both *mitfa* and *colony stimulating factor-1 receptor a* (*csf1ra*), respectively (Frohnhofer et al. 2013; Gur et al. 2020; Lister et al. 1999) (Figure 1b, upper). In the fins, pigment cells were either missing entirely, or iridophores were present in numbers markedly fewer than wild-type (Figure 1b, lower; Figure S1d).

To learn if other neural crest-derived cell types were affected, we examined embryos carrying fluorescent reporters for neurons (nbt), multipotent progenitors and glia (*sox10*), melanoblasts and xanthoblasts (*mitfa*), late melanoblasts and melanophores (*tyrp1b*), and xanthoblasts and xanthophores (*aox5*). *varo* homozygotes had marked deficiencies in *mitfa*+, *tyrp1b*+ and *aox5*+ cells suggesting effects specific to melanophore and xanthophore development (Figure 2). By young adult stages, *varo* homozygotes had acquired variably sized populations of unpigmented *mitfa*+ cells, as well as unpigmented and abnormally stellate cells expressing low levels of *aox5* (Figure S2). Given deficiencies in these cells during embryogenesis, differentiation-arrested *mitfa*+ and *aox5*+ cells of adults may derive from latent, post-embryonic progenitor pools (McMenamin et al. 2014; Parichy and Turner 2003; Singh et al. 2016). The combined phenotypes of *varo*—reduced pigmentation and pattern disturbance in heterozygotes along with absence of pigmented melanophores and xanthophores in homozygotes—have not been reported previously.

3.2 | *varo* Is An Allele of *mitfa* and Affects the Survival of Embryonic *mitfa*+ Cells

We sought to identify the *varo* locus by whole-genome resequencing and association mapping. These analyses placed *varo* on chromosome 6 in the vicinity of *mitfa* (Figure 3a), suggesting *varo* might be an allele of *mitfa* and consistent with defects in the development of cells expressing the *mitfa* reporter and the derivatives of these cells. Indeed, map-cross sequencing and targeted Sanger sequencing revealed two novel *mitfa* coding sequence variants (Figure 3b). The affected amino acid for one variant, His204Arg, occurs in the basic region of the DNA binding domain and is predicted to be deleterious [SIFT score 0.00; (Ng and Henikoff 2003)]; the other amino acid, Gly355Ser, is near the C-terminus and is likely tolerated (SIFT score 0.82).

Remarkably, two semi-dominant ENU-induced alleles of *Mitf* in mice, *Mitf*$^{mi\text{-}enu5}$ and *Mitf*$^{mi\text{-}bcc2}$ exhibits the same nucleotide (a → g) and amino acid substitution as His204Arg, at the corresponding site, His209Arg (Figure 3c,d) (Hansdottir et al. 2004). The mouse alleles have dilute coat color as heterozygotes and

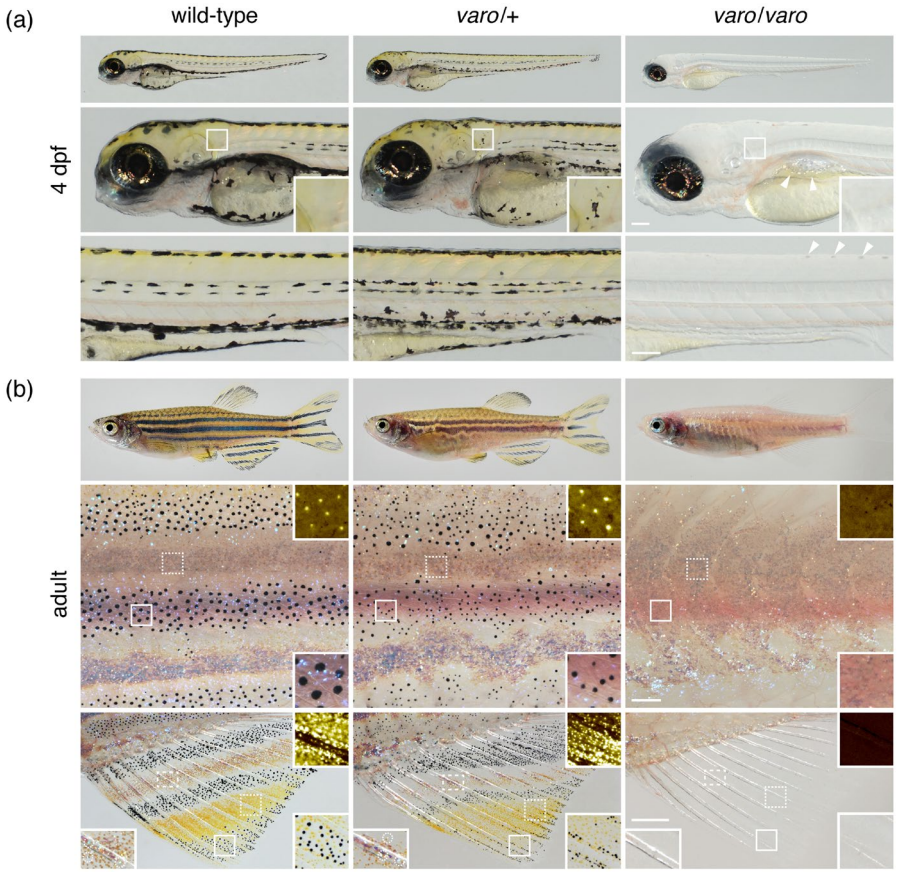

FIGURE 1 | Phenotypes of *varo* mutant. (a) Early larvae had irregular patterns of melanophores if heterozygous and lacked melanophores and xanthophores if homozygous. Insets show normal yellow color from xanthophores, posterior to otocyst, ectopic and hypomelanized melanophores, with yellow color of xanthophores in heterozygote and absence of melanophores and xanthophore color in homozygote. Arrowheads, persisting iridophores in normal locations in the homozygote, as a sheet of cells above the swim bladder and as individual cells along dorsal midline. Counts of dorsal iridophores did not differ among wild-type, heterozygous or homozygous siblings ($F_{2,36} = 1.07$, $p = 0.4$). (b) Adult heterozygotes had irregular stripes with melanophores that contained less melanin than the wild type, whereas homozygotes lacked stripes as well as melanophores and xanthophores. Details of flanks and fins are shown after treating with epinephrine to contract pigment granules towards cell centers. Flank insets: Details of areas outlined by dashed squares show pseudocolored xanthophores in bright yellow–orange on a dark background (Figure S1a); details of areas outlined by solid squares illustrate melanophores, iridophores (iridescent or purplish grey) or both. Fin insets: Dashed squares, pseudocolored xanthophores; solid squares, melanophores and xanthophores; dashed rectangles, iridophores (iridescent or purplish, examples circled), and xantholeucophores (orange–brown). Scale bars: A, 100 μm; b, 200 μm flank, 500 μm fin.

completely lack melanocytes as homozygotes, similar to hypomelanization of melanophores in *varo*/+ and absence of melanophores in *varo*−/−. This concordance implies that *varo* has a functionally significant *mitfa* mutation and is consistent with the suggestion of a mutational hotspot at this site (Hansdottir et al. 2004). An identical single nucleotide polymorphism occurs in humans (rs1553704093) and is presumed to be pathogenic (Accession: VCV000432664.2).

While there are similarities between *varo* and mouse phenotypes, *varo* differs from *mitfa*^{w2} of zebrafish, which contains a premature termination codon: *mitfa*^{w2} is recessive and develops xanthophores even when homozygous (Lister et al. 1999). We therefore considered the possibility that *varo* might have a second-site mutation in a closely linked gene. This model would be excluded if the introduction of a premature termination codon into *mitfa* of *varo* were to restore recessivity and xanthophores, as in *mitfa*^{w2}. To test this prediction, we induced a frame-shift leading to a premature termination codon upstream of the *varo mitfa* mutations. Fish heterozygous for the resulting allele (*mitfa*^{vp70rc1varo}, *mitfa*^{rc1varo}; Figure S3a) lacked discernible phenotypes, whereas fish homozygous for this allele developed xanthophores (Figure 3b,e). We conclude that *varo* corresponds to *mitfa*, rather than *mitfa* and an additional locus.

To further assess the differing phenotypes of wild-type, *mitfa*^{varo}, and *mitfa*^{w2} we examined *mitfa*+ cells by time-lapse as well as super-resolution imaging during neural crest dispersal and embryonic pigment cell development. Analyses of *mitfa*^{varo} homozygotes revealed a substantially increased incidence of cell death and fewer persisting cells overall (Figure 4; Figure S4; Movies S1–S4), consistent with the deficits in *mitfa*+ cells as well as *tyrp1b*+ and *aox5*+ cells by 72 hpf (Figure 2a). By comparison, *mitfa*^{w2} homozygotes had migratory behaviors similar to wild-type and only mild defects in cell survival. These observations further demonstrate the severity of the *varo* phenotype relative to that of the premature termination codon, loss-of-function allele.

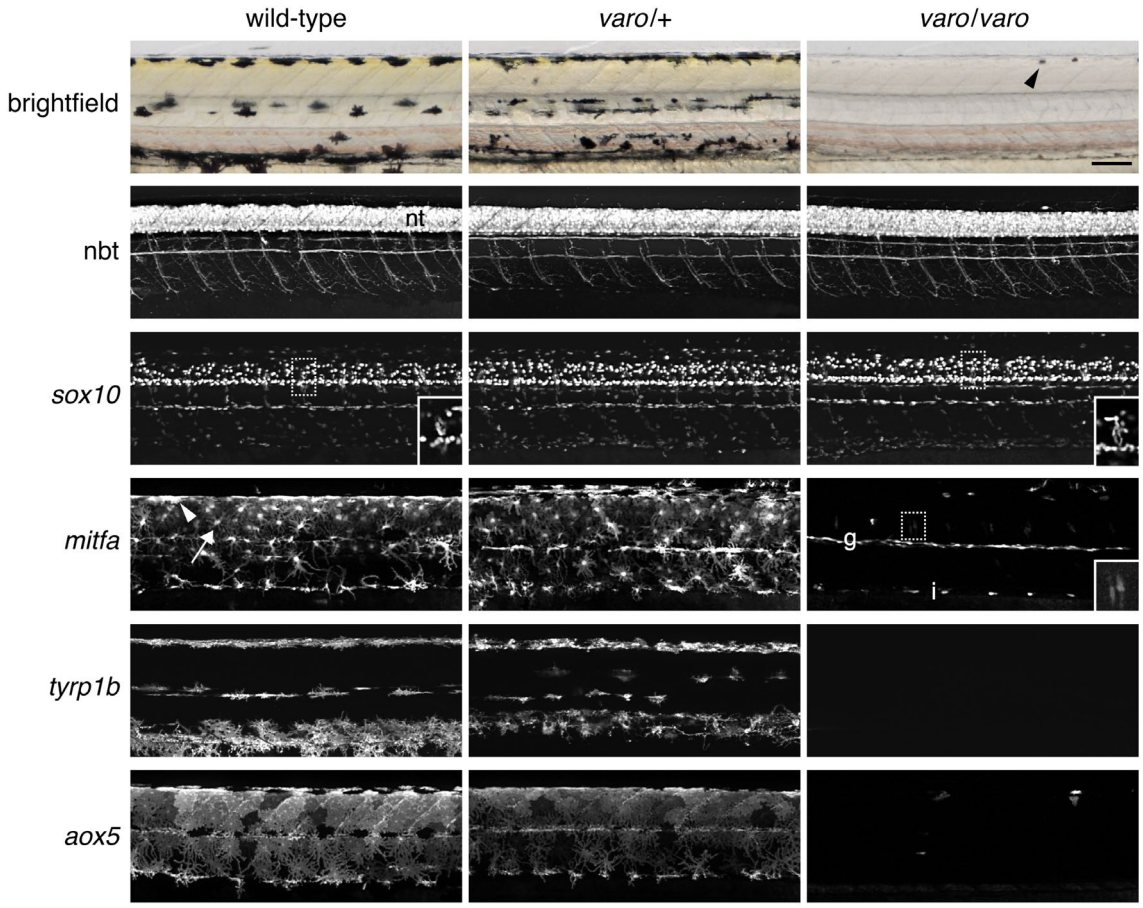

FIGURE 2 | *varo* affects developing melanophores and xanthophores. Brightfield and fluorescent reporter lines in wild-type and *varo* mutant siblings at 72 h post-fertilization (hpf). For each reporter, all genotypes were imaged with the same acquisition times, with extended focus projections shown except where indicated. nbt:DsRed and *sox10*:Eos expression in the neural tube (nt) and peripheral nervous system were indistinguishable among genotypes. Insets show single focal plane details of *sox10*+ cells in the dorsal root ganglia. *mitfa*:Eos, like *mitfa* transcript (Lister et al. 1999; Parichy et al. 2000), was detectable in wild-type melanophores (e.g., arrowhead), xanthophores (arrow), and their precursors. In *varo*−/− mutants, few *mitfa*+ cells were present. The inset shows two faint *mitfa*+ cells near the dorsal root ganglia at a higher display value. g, *mitfa*+ glia along the lateral line nerve; i, presumptive *mitfa*+ iridophores, which also exhibit detectable *mitfa* transcript. *tyrp1b*:PALM-mCherry marked melanophores and melanoblasts in wild-type and *varo*/+, but *tyrp1b*+ cells were missing in *varo*/*varo*. *aox5*:PALM-EGFP marked xanthophores and xanthoblasts, with *aox5* cells mostly absent in *varo*/*varo*. The arrowhead in the brightfield image of *varo*/*varo* indicates one of two visible iridophores, which appear dark in the transmitted illumination used here. Scale bar: 100 μm.

3.3 | Mitfa Dominant Negative Impact on Xanthophore Development

We wished to understand why $mitfa^{varo}$ and the premature termination alleles differ in their phenotypes, especially with respect to xanthophore complement. To this end, we considered the formal possibility that *mitfa* is not only expressed in xanthophores (Parichy et al. 2000) but is required for their development. If so, the persistence of xanthophores in premature termination alleles could reflect genetic compensation that fails to occur in $mitfa^{varo}$. This might be the case if nonsense-mediated decay of premature termination mRNAs leads to transcriptional adaptation at other loci (El-Brolosy et al. 2019; Kontarakis and Stainier 2020).

To test this model, we circumvented the possibility of nonsense-mediated decay by generating a deletion allele ($mitfa^{vp70rc2del}$, $mitfa^{del}$) that fails to produce transcript (Figure 3b; Figure S3b). Homozygotes developed numerous xanthophores (Figure 5a), showing that *mitfa* alone is not essential for xanthophore development and making transcriptional adaptation an unlikely explanation for xanthophore persistence in the premature termination alleles. Early larvae homozygous for $mitfa^{del}$ also developed about twice as many iridophores as wild-type or *varo* mutants, qualitatively similar though numerically greater than the excess iridophores of early larvae homozygous for $mitfa^{w2}$ (Lister et al. 1999), and significantly more iridophores than $mitfa^{varo}$ (Figure S5). The deletion allele also lacked discernible phenotypes when heterozygous, confirming the haplo-sufficiency of Mitfa in zebrafish—similar to mouse—but contrasting with haploinsufficiency in human and hamster (Hodgkinson et al. 1998; Steingrimsson et al. 1994; Tachibana 1997).

An alternative explanation for the severity of $mitfa^{varo}$ is dominant negative activity. Indeed, His204Arg occurs in the basic region of the DNA binding domain, where semi-dominant and dominant negative effects are evident for other mutations, including His209Arg of mouse, which also has ~2.5-fold reduced

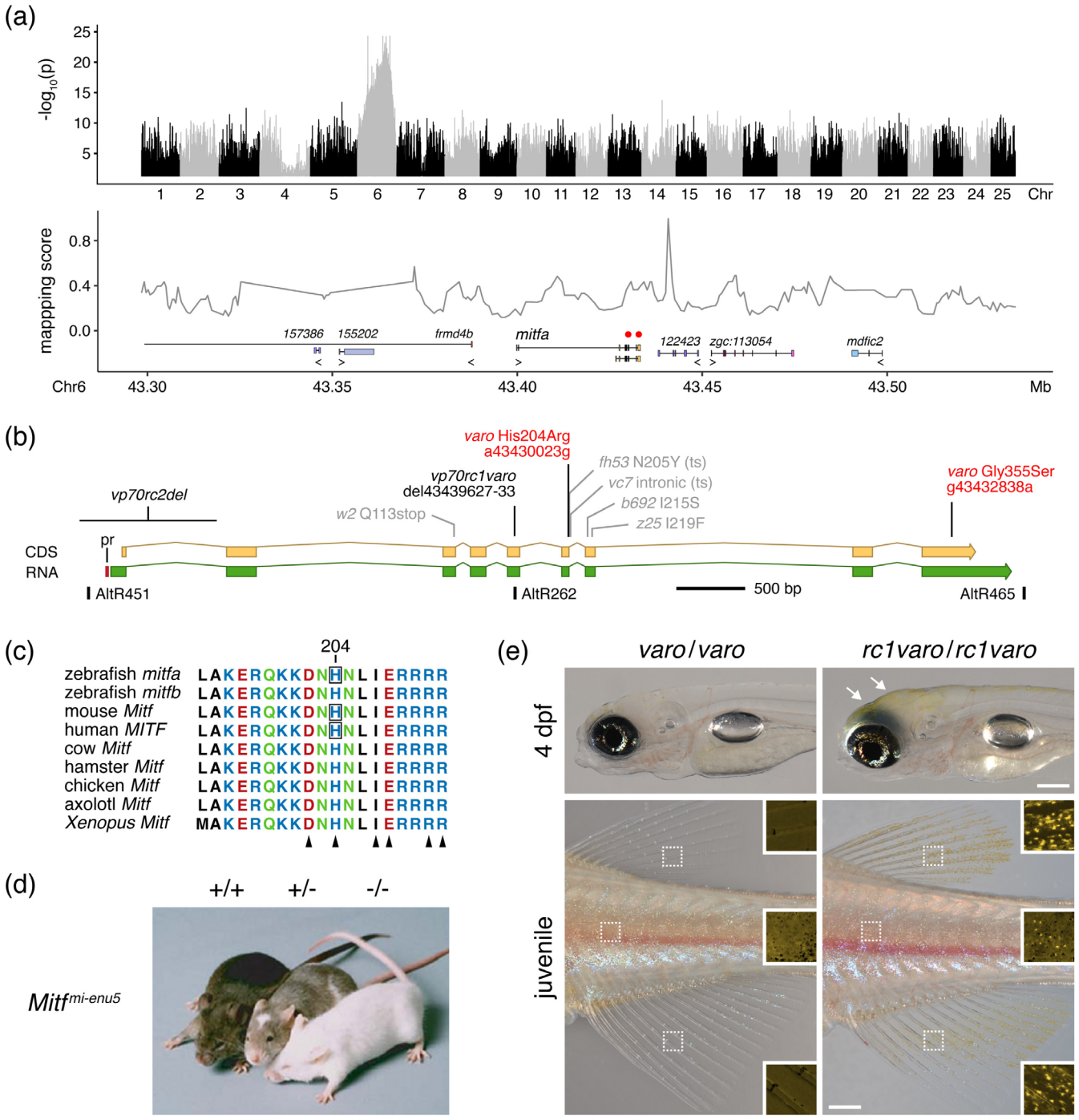

FIGURE 3 | *varo* is allelic to *mitfa*. (a) Association mapping by whole-genome resequencing placed *varo* on Chr6 in the vicinity of *mitfa* (upper). Only two potentially deleterious variants were identified (red circles, lower), both perfectly associated with phenotype and both in exons of *mitfa*. Numbered, anonymous loci indicate Ensembl transcript identifiers (ENSDART...). (b) Two missense substitutions in *varo* are shown in red (nucleotide coordinates reference GRCz11). Additional alleles generated in this study are shown in black (see main text), and previously identified alleles (Johnson et al. 2011; Lister et al. 2001, 1999) are shown in grey (ts, temperature sensitive). The locations of AltR CRISPR/Cas9 targets are shown below the gene body with AltR451, AltR465 used to generate a deletion allele (see main text). pr, conserved promoter element (Baranasic et al. 2022) (c) Alignment illustrating near-invariance of the basic region of the DNA-binding domain across species. Sequence translation from the second zebrafish Mitf gene, *mitfb*, is included. Histidine residues are boxed for species reported to have ENU-induced or natural His→Arg missense substitutions, as in *varo*. Arrowheads indicate sites of missense mutations with dominant negative activities (Hallsson et al. 2000; Hansdottir et al. 2004; Hemesath et al. 1994; Philipp et al. 2011; Yamamoto et al. 2024). (d) Mice that are wild-type, heterozygous or homozygous for an H209R allele (reproduced with permission from Hansdottir et al. 2004). (e) Homozygous *varo* and homozygous *varo* with premature termination codon ($mitfa^{vp70rc1varo}$, 7 base pair deletion leading to 11 novel amino acids followed by a stop codon). Introduction of a non-sense mutation on the *varo* background restored xanthophores in larvae (arrowheads) and adults (insets) when homozygous and abolished semi-dominance when heterozygous ($mitfa^{vp70rc1varo}$/+). Dark spots in insets are due to iridophore iridescence. Scale bars: Upper, 200 μm; lower, 500 μm.

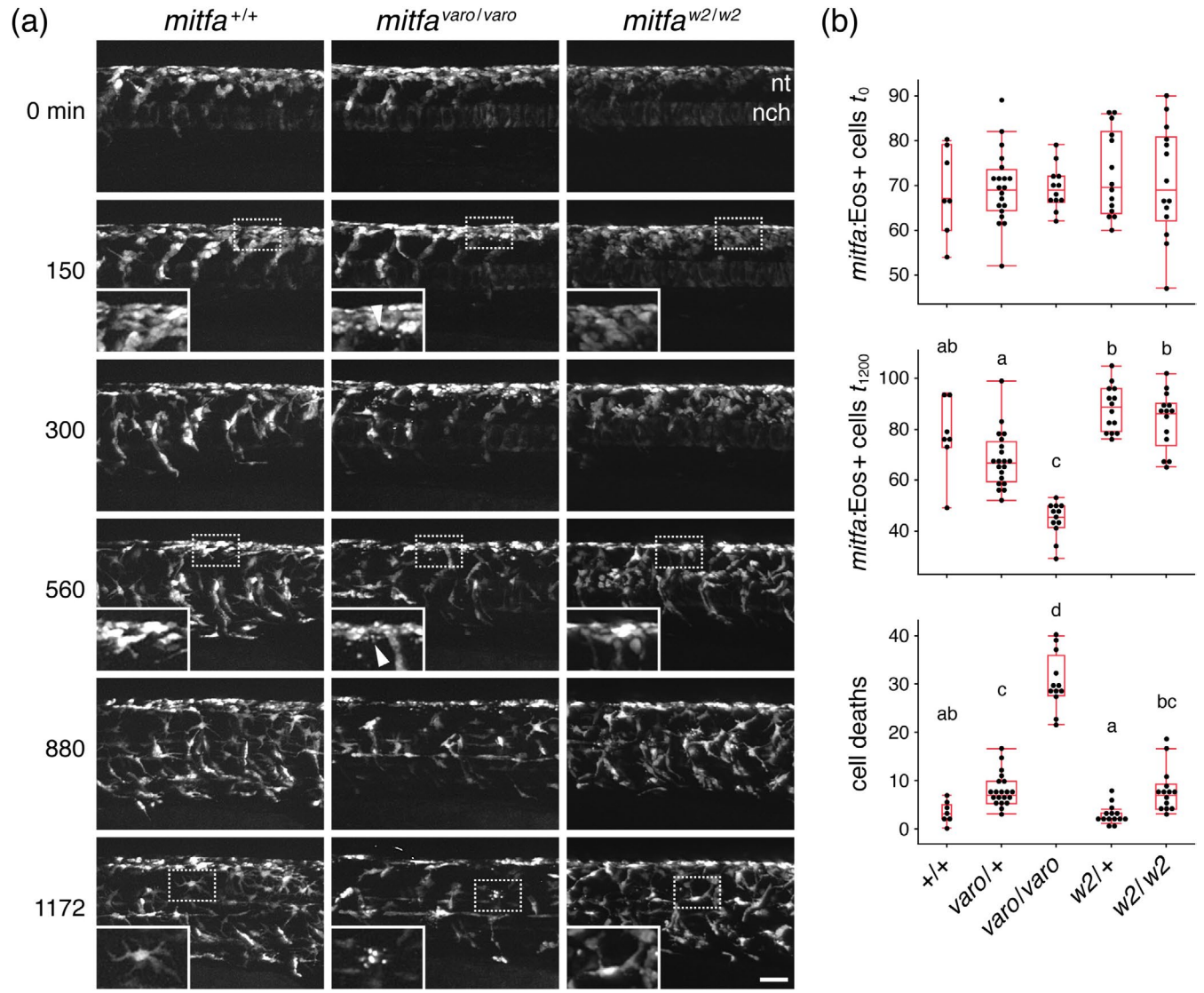

FIGURE 4 | Time-lapse imaging reveals the death of *mitfa*:Eos+ cells in *varo* mutants. (a) Example image series from wild-type and homozygous mutant *varo* siblings, as well as a *mitfa*^{w2} homozygous mutant, imaged at the level of the posterior yolk extension for 20 h beginning at 22 h post-fertilization. nt, level of neural tube. nch, notochord (weakly fluorescent with this reporter). Insets show normal morphologies of cells in wild-type and *mitfa*^{w2}, and cellular debris (arrowheads) present from early time points in all *varo* mutants. Such debris was also apparent in embryos not subjected to time-lapse imaging (Figure S4). (b) Box plots show reduced numbers of *mitfa* + cells in *mitfa*^{varo} heterozygotes and homozygotes, as compared to wild-types and *mitfa*^{w2} at the end of imaging (overall Kruskal–Wallis $\chi^2 = 42.4$, 4 df, $p < 0.0001$), without significant differences at the beginning of imaging ($\chi^2 = 0.6$, 4 df, $p = 0.9$). Differences were associated with an incidence of cell death (lower plot) markedly greater in *varo*−/− than in other genotypes ($\chi^2 = 45.9$, 4 df, $p < 0.0001$). Shared letters above groups indicate medians not significantly different from one another ($p > 0.05$) in *post hoc* comparisons (non-parametric Steel-Dwass method). $N = 67$ embryos, using sibling *mitfa*$^{+/+}$, *mitfa*$^{varo/+}$ and *mitfa*$^{varo/varo}$, and sibling *mitfa*$^{w2/+}$ and *mitfa*$^{w2/w2}$. The scale bar: 50 μm.

affinity for M-box and E-box motifs and reduced DNA-binding specificity overall (Hansdottir et al. 2004; Pogenberg et al. 2012; Steingrimsson et al. 1994). In zebrafish, the dominant negative effects of Mitfa^{varo} on wild-type Mitfa plausibly explain the hypomelanization of melanophores in heterozygotes. Impacts on other factors could explain the loss of xanthophores in homozygotes.

As a first step in testing the idea that interactions of mutant Mitfa with other factors lead to phenotypes beyond *mitfa* loss-of-function, we examined *mitfa*^{vc7}, inferred to have dominant negative activity resulting from a temperature-sensitive splicing defect that can generate an in-frame truncation of the DNA binding domain (Johnson et al. 2011; Zeng et al. 2015) (Figure 3b). We therefore predicted that *mitfa*^{vc7} homozygotes should have reduced xanthophore pigmentation, reminiscent of *mitfa*^{varo}. Indeed, larvae homozygous for *mitfa*^{vc7} had marked deficiencies in xanthophore pigmentation (Figure S6).

3.4 | Genetic Interactions of Mitfa in Xanthophore and Iridophore Development

Given the xanthophore defect in a second presumptively dominant negative allele, we reasoned that: (i) Mitfa likely collaborates with another factor in xanthophore progenitors; and (ii)

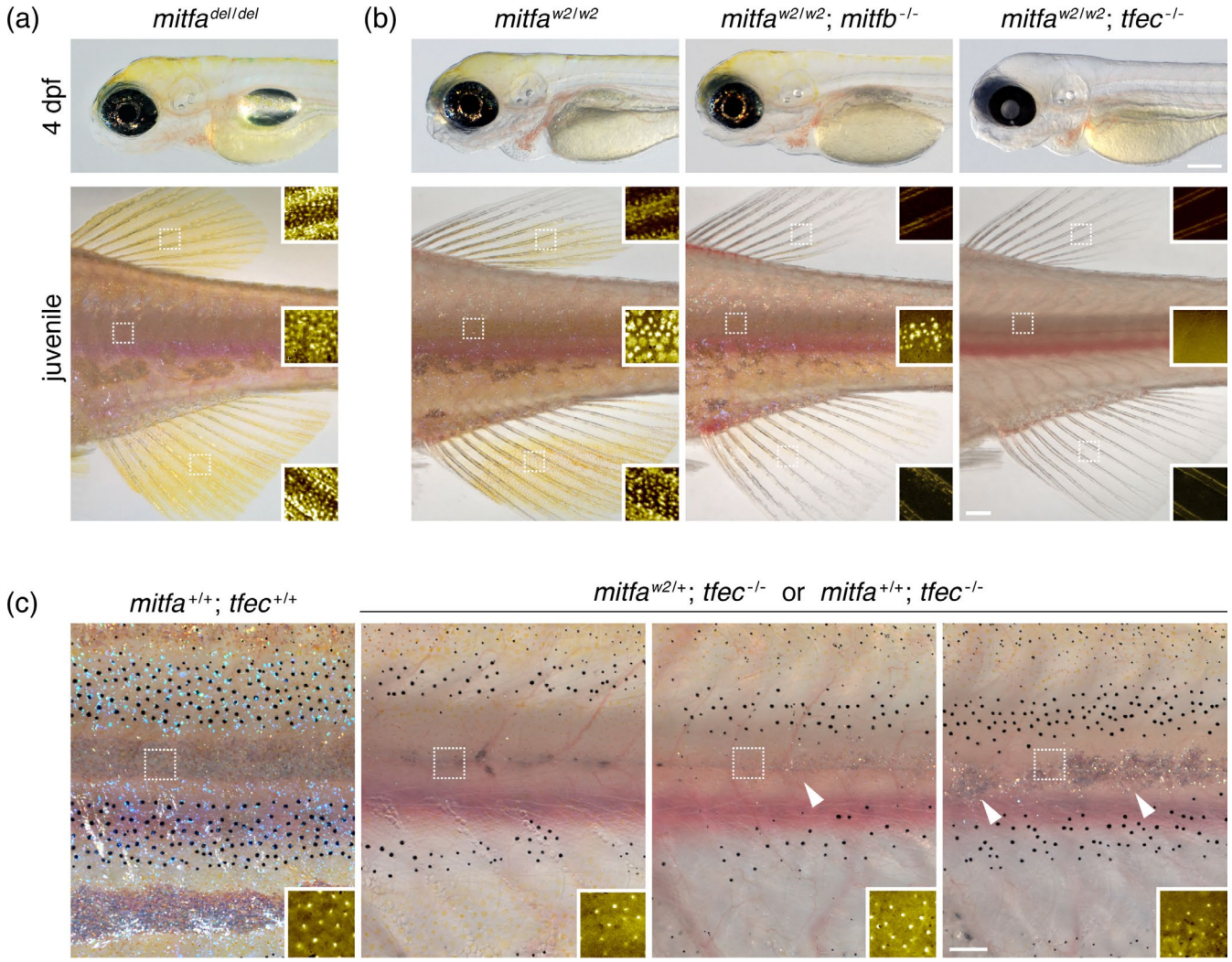

FIGURE 5 | Deletion and double mutant analyses suggest interactions of Mitfa with other bHLH-ZIP MiT subfamily members. (a) Mutants homozygous for a deletion (*mitfa*^{del}) that prevents *mitfa* transcription developed abundant embryonic and adult xanthophores. (b) Double mutants for *mitfa*^{w2} and *mitfb* developed xanthophores, albeit fewer in the adult than *mitfa*^{w2} single mutants, with this deficit noticeable especially in fins. Double mutants for *mitfa*^{w2} and *tfec* completely lacked xanthophores in early larvae. *tfec* mutants were semi-viable through later larval stages owing to defects in swim bladder development and potentially other traits, but surviving *mitfa; tfec* mutant juveniles and adults lacked xanthophores, despite their presence in *tfec* single mutants (Petratou et al. 2021) (e.g., Figure S8b,c). (c) *tfec* homozygotes often recovered adult iridophores if wild-type or heterozygous mutant for *mitfa*. The left panel shows wild-type and three right panels show variable complements of iridophores in sibling *tfec*−/− fish with one or two *mitfa*$^{+}$ alleles (individuals with iridophores: *mitfa*^{w2}/+, 4 of 7 genotyped; *mitfa*+/+, 2 of 3 genotyped). Whole-fish images of adults are also shown in Figure S8a. Scale bars: For a and b, upper 200 μm, lower 500 μm; c, 250 μm.

candidate interacting factors should be identifiable by xanthophore deficiencies similar to *mitfa*^{varo} in fish doubly mutant for the interacting locus and *mitfa*^{w2}. A priori candidates would include the product of the paralogous locus, *mitfb* (Lister et al. 2001), with which Mitfa could reasonably be expected to form heterodimers, as well as other closely related bHLH-ZIP, MiT subfamily transcription factors with which MITF of mouse can heterodimerize (Hemesath et al. 1994). Transcripts of each of the orthologous loci are detectable in one or more pigment cell or progenitor lineages, and at one or more stages of development (Figure S7a,b) (Lister et al. 2011).

Among MiT subfamily genes, we sought to test roles specifically for *mitfb* and *tfec*, given prior associations of these loci with pigmentation. A null allele of *mitfb* develops an apparently normal complement of melanophores and xanthophores (Lane and Lister 2012) but early larvae simultaneously mutant for *mitfa* and *mitfb* are reported to be xanthophore-deficient (Miyadai et al. 2023). *mitfb* transcripts are detectable in xanthophores by some but not other analyses (Figure S7a,b) (Lister et al. 2011). *tfec* is expressed robustly in pigment cell progenitors and iridophores and at lower levels in melanophores, xanthophores, or their specified precursors during embryogenesis and adult pigment pattern formation (Figure S7a,b) (Lister et al. 2011; Petratou et al. 2021). Combined transcript counts are greater for pigment cell progenitors co-expressing *mitfa* and *tfec* than for *mitfa* and other candidates (Figure S7a,b). *tfec* mutants are reported to lack iridophores; though embryos and adults develop melanophores and xanthophores, both are delayed in their specification (Petratou et al. 2021). Exogenously supplied Mitfb and Tfec can each rescue melanophores to some degree in *mitfa*^{w2} mutants (Lister et al. 2001;

Petratou et al. 2021), revealing overlap in potential activities across MiT subfamily members.

To test for interactions with Mitfa and the phenocopy of the *mitfa*^{varo} xanthophore loss, we generated premature termination alleles of *mitfb* and *tfec* (Figure S3a) and bred them to homozygosity in the background of *mitfa*^{w2}. Mutants for *mitfa*^{w2}; *mitfb* developed xanthophores in early larvae and in juveniles, though xanthophores of juveniles and adults were fewer, less pigmented, and developed more slowly than in *mitfa*^{w2}, with xanthophores of the fins especially impacted (Figure 5b; Figure S8a). By contrast, mutants for *mitfa*^{w2}*; tfec* lacked xanthophores in embryos through adults, despite mutants for *tfec* alone developing xanthophores after a ~1 day delay (Figure 5b; Figure S8b,c) consistent with the transient impediment to specification inferred previously (Petratou et al. 2021).

Finally, we observed additional interactions that affected iridophores. Fish homozygous mutant for *tfec*, or doubly homozygous mutant for *mitfa*^{w2} and *tfec*, completely lacked iridophores at early larval stages, as expected (Petratou et al. 2021); *mitfa*^{w2}*; tfec* double mutants were similarly devoid of iridophores through later larval stages and in the adult (Figure 5b; Figure S8a). Yet we found that *tfec* homozygotes could recover variable numbers of iridophores during the development of the adult pigment pattern, provided they were also carrying one or two wild-type *mitfa* alleles (Figure 5c; Figure S8a).

Together these findings reveal genetic interactions between *mitfa* and *tfec*, support a model in which Mitfa and Tfec together promote xanthophore development, and point to the likelihood of compensation among MiT-subfamily members.

4 | Discussion

The neural crest and its many derivatives are a classic and enduring model of cell fate specification. Our analyses, beginning with the *varo* mutant allele of *mitfa*, provide insights into genetic requirements for neural crest-derived pigmentary fates and point to previously undocumented roles for Mitfa and other MiT subfamily bHLH-ZIP transcription factors in these processes.

An ortholog of mammalian *MITF*, the master regulator of melanocyte development (Goding and Arnheiter 2019), zebrafish *mitfa* has been well studied since a mutant allele, *mitfa*^{w2} (*nacre*^{w2}), was identified by forward genetics for its lack of melanophores in embryos through adults (Lister et al. 1999). The first 25 years of *mitfa* studies identified regulatory requirements (Curran et al. 2009; Dorsky et al. 2000; Elworthy 2003; Petratou et al. 2018; Vibert et al. 2017), functions in melanophore development and homeostasis (Gur et al. 2020; Johnson et al. 2011; Kenny et al. 2022; Taylor et al. 2011), and activities in melanoma (Dilshat et al. 2021; Lister et al. 2014; Louphrasitthiphol et al. 2020), many of which parallel or likely parallel those of mammalian MITF genes (Goding and Arnheiter 2019; Vu et al. 2021). Broad concordance between *mitfa* and avian Mitf genes is apparent as well (Minvielle et al. 2010; Zhou et al. 2018).

The elaborate pigmentary systems of teleosts and other ectotherms provide opportunities to learn how Mitf genes are integrated into the developmental programs of additional pigment cell types, and whether such functions are conserved evolutionarily. In the first description of *mitfa*^{w2}, xanthophore pigmentation was considered to be somewhat reduced in embryos and early larvae and variable in adults (Lister et al. 1999). These observations, and the expression of *mitfa* and its transcriptional reporters in xanthophores and their progenitors (Eom et al. 2012; Parichy et al. 2000) (Figure S5), suggested a potential involvement, though not an absolute requirement, in embryonic and adult xanthophore lineages. The most notable outcome of this study is to implicate interactions between *mitfa* and *tfec* in xanthophore development. The possibility of Mitfa interacting with additional factors was suggested by fish mutant for *varo*, which we showed to have a missense mutation affecting the basic region of the Mitfa DNA binding domain, where mutations are known to elicit dominant negative activity (Hansdottir et al. 2004; Pogenberg et al. 2012). Interference of Mitfa^{varo} with wild-type Mitfa in heterozygotes was suggested by reduced pigment in melanophores, body stripe irregularities, and lack of fin melanoleucophores (Huang et al. 2025; Lewis et al. 2019). Interaction with the product of another locus was suggested by: (i) the absence of embryonic and adult xanthophores in *mitfa*^{varo} homozygotes, different from *mitfa* loss-of-function alleles; (ii) the phenocopy of this xanthophore defect by simultaneous homozygosity for premature termination alleles of *mitfa* and *tfec*; and (iii) the exclusion of transcriptional adaptation by nonsense-mediated decay as an explanation for persisting xanthophores in premature termination alleles.

Collaboration between *mitfa* and *tfec* in xanthophore development—inferred genetically—could reflect several possible molecular and cellular mechanisms. One appealing scenario would invoke sequential and partially redundant activities, suggested already by prior observations. Transcripts of *tfec* are detected in premigratory and migratory neural crest cells, and transcripts for *mitfa* are evident in some of these cells shortly thereafter. Later, *tfec* expression drops substantially in melanoblasts that have high *mitfa* expression, drops moderately in xanthoblasts with moderate *mitfa* expression, and increases to high and stable levels in iridoblasts and iridophores, with little or no *mitfa* expression (Lister et al. 2011, 1999; Petratou et al. 2021, 2018) (Figure 5a,b). Similar dynamics are evident post-embryonically (Saunders et al. 2019). These reciprocal changes in gene expression are consistent with *mitfa*-dependent repression of *tfec*, as is true for the orthologous loci in mouse retinal pigmented epithelium (Bharti et al. 2012); a still-unknown factor that mediates Tfec-dependent downregulation of *mitfa* has been hypothesized (Petratou et al. 2021). Despite this apparent repression, Tfec can substitute for Mitfa experimentally in rescuing zebrafish melanophores, and MITF can substitute for TFEC in mouse retinal pigmented epithelium (Bharti et al. 2012; Petratou et al. 2021). Whether potential heterodimers of these factors during periods of overlapping expression interact with the same suite of target genes as homodimers or have subsets or even unique targets would be interesting to learn.

Prior observations and our own analyses thus suggest a model in which early Tfec functions in promoting chromatophore specification are handed off to Mitfa, with Mitfa contributing to later steps in specification and differentiation, and also to *tfec* downregulation in xanthophore and melanophore lineages. The

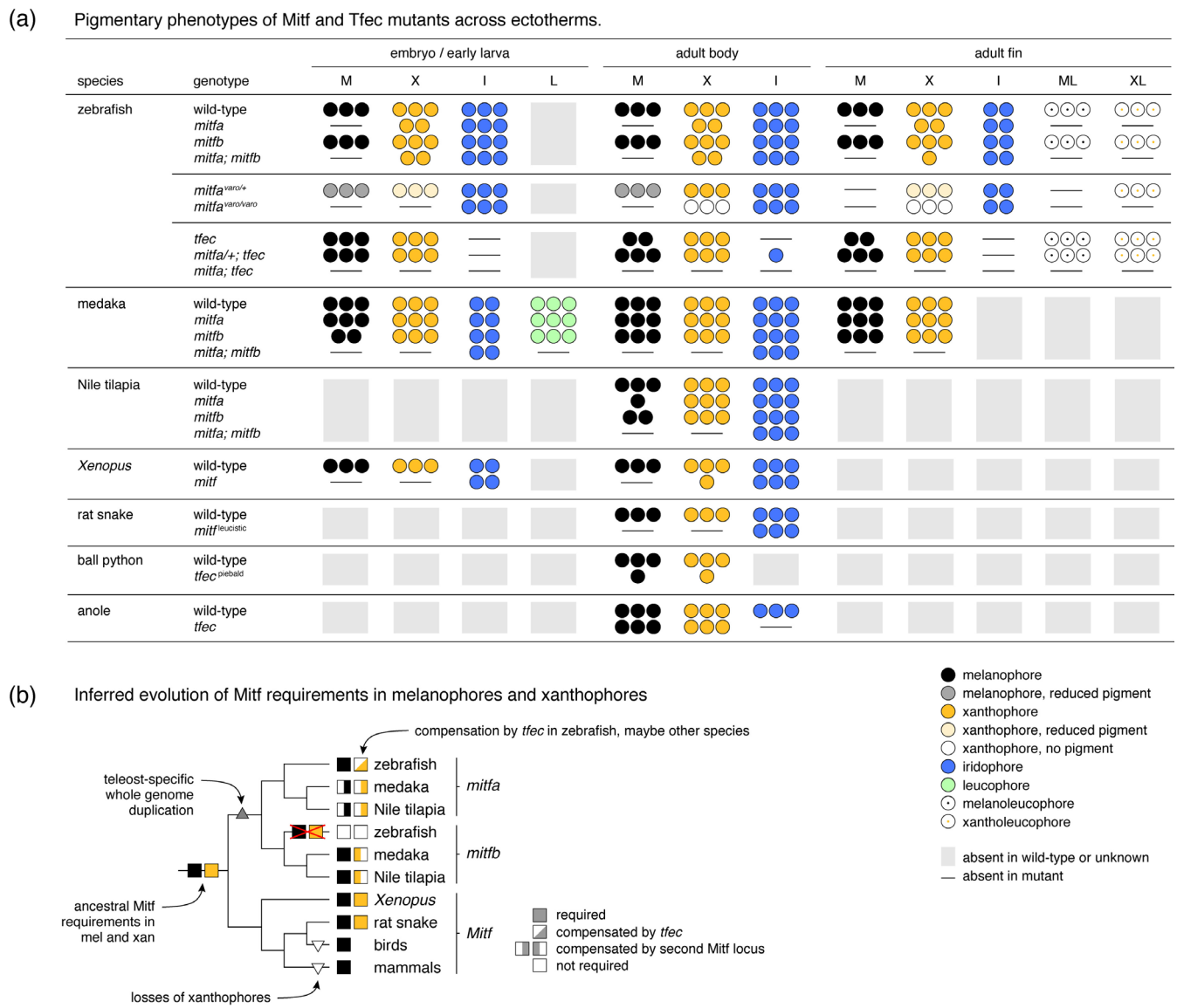

FIGURE 6 | Pigmentary phenotypes of Mitf and Tfec mutants and inferred evolution of Mitf requirements. (a) Several studies have now examined phenotypes resulting from Mitf or Tfec mutation. Summary illustrates for indicated pigment cell classes absences, reduced numbers or changes in states across life stages and anatomical locations when relevant and described (this study; Garcia- Elfring et al. 2023; Lane and Lister 2012; Lister et al. 1999; Miyadai et al. 2023; Ran et al. 2024; Tzika 2024; Ullate-Agote and Tzika 2021; Wang et al. 2021). Reduced numbers of cells indicated by fewer symbols are not intended to be quantitative. Key shown at lower right. (b) Observations available so far suggest an ancestral vertebrate requirement for Mitf in both melanophores and xanthophores. With an additional whole-genome duplication in teleosts, Mitf continued to be required but loss of one Mitf locus could be compensated by another. Only in zebrafish has one Mitf locus, *mitfb*, undergone a substantial, though not complete (Figure 5b) reduction in pigmentary function (loss of requirements by melanophores and xanthophores marked with red X), with compensation for *mitfa* loss from the more distant MiT subfamily member gene, *tfec*, and only to a lesser extent *mitfb*.

absence of Mitfa, as in a premature termination or deletion allele, would thus lead to de-repression of *tfec*, and promiscuity in Tfec transactivation would largely, but not completely, compensate for the loss of Mitfa—consistent with the somewhat diminished xanthophore pigmentation of $mitfa^{w2}$. Conversely, the absence of Tfec would be compensated for by the later, *tfec*-independent onset of *mitfa* expression, allowing xanthophore lineage development to proceed, concordant with the late appearance of xanthophores observed here, and delayed specification observed previously (Petratou et al. 2021). For a dominant negative Mitfa ($Mitfa^{varo}$ or $Mitfa^{vc7}$), dimerization with wild-type Mitfa would impact melanophores leading to the heterozygous, semi-dominant phenotype; heterodimerization with Tfec (Hemesath et al. 1994) would inhibit Tfec activities including its potential to compensate for Mitfa, impacting both melanophores and xanthophores and likely causing the death of progenitors as observed by time-lapse imaging. Though plausibly explaining the phenotypes described here, this model has caveats: it has not yet been possible to assess the co-occurrence of Mitfa and Tfec or their heterodimerization in vivo, whether functionally significant interactions occur with other MiT subfamily members, or the extent to which homodimers and potential heterodimers transactivate the same or different sets of target genes.

Beyond xanthophores, our analyses revealed an unexpected interaction in later larvae and adults: homozygous mutants for *tfec* could recover a variable complement of adult iridophores when carrying one or two wild-type alleles of *mitfa*. This outcome also fits with compensatory effects and overlap in target genes, including the guanine synthesis gene *pnp4a* (Petratou et al. 2018), important for iridophore reflecting platelet formation. We speculate that in *tfec* mutants, the presence of wild-type Mitfa allows multipotent progenitors to respond to signals for iridophore differentiation that are likely abundant in the interstripe region (Frohnhofer et al. 2013; Patterson and Parichy 2013). The failure of *mitfa* to compensate for *tfec* loss in the development of early larval iridophores might reflect autonomous differences between sublineages of iridophore-forming progenitors (Budi et al. 2011; Curran et al. 2010; Petratou et al. 2018; Singh et al. 2016), the relatively brief developmental window in which early larval iridophores form as compared to the more protracted period of adult pattern formation (Lopes et al. 2008; Parichy et al. 2009; Patterson and Parichy 2013), or other factors.

Independent of *tfec* effects, we additionally found that variation in early larval iridophore complements across *mitfa* alleles, consistent with the initial report of ~40% more of these cells in *mitfa*^{w2} than wild-type (Lister et al. 1999). Excess early larval iridophores in *mitfa*^{w2} and the deletion allele *mitfa*^{del} could reflect transfating of progenitors that would otherwise develop as melanophores; quantitative differences in iridophore excess between these alleles might reflect genetic background or allele-specific differences. By contrast, the numbers of early larval iridophores were normal in *mitfa*^{varo} heterozygotes and homozygotes. We speculate that this outcome reflects dominant negative effects of Mitfa^{varo} that partially interfere with Tfec, reduced survival of progenitors that limits the pool of cells that might differentiate as iridophores, or both of these factors.

Whereas interactions between *mitfa* and *tfec* were most substantial, we also uncovered an interaction involving the second Mitf gene of zebrafish, *mitfb*, which is not required on its own by xanthophores (Lane and Lister 2012; Lister et al. 2001). Early larvae mutant for both *mitfa*^{w2} and *mitfb* resembled those for *mitfa*^{w2} alone. By adult stages, however, *mitfa*^{w2}*; mitfb* fish were more deficient than *mitfa*^{w2} for xanthophore pigmentation on body and even more severely compromised for xanthophores in the fins. These phenotypes suggest that *mitfb* partially compensates for the loss of *mitfa* (though not *tfec*) in xanthophores and especially so in the fins. Our findings differ somewhat from Miyadai et al. (2023), in which embryos and early larvae doubly mutant for *mitfa*^{w2} and *mitfb* alleles with truncations in the DNA binding domain had deficiencies in xanthophores; adult phenotypes were not reported. Overall, however, our analyses and those of Miyadai et al. (2023) support the idea that Mitf gene dosage impacts xanthophores and point to differential sensitivities of xanthophore subpopulations across stages and anatomical locations.

Finally, our analyses, in combination with prior studies of other species, allow insights into evolutionary aspects of MiT subfamily roles in pigmentation (Figure 6). For example, zebrafish *mitfa* mutations lead to the complete loss of melanophores, with only minor additional defects resulting from dual *mitfa* and *mitfb* mutations. In medaka, however, *mitfa* single mutants lack discernible phenotypes, *mitfb* mutants have a transient delay in early larval melanophore development, and *mitfa; mitfb* double mutants lack melanophores, xanthophores, and leucophores (Miyadai et al. 2023). In tetrapods, *Xenopus tropicalis* mutants for the single Mitf gene lack both melanophores and xanthophores, as do leucistic rat snakes (Ran et al. 2024; Ullate-Agote and Tzika 2021). These and other phenotypes indicate the phylogenetic generality of MiT subfamily requirements in multiple pigment cell lineages and suggest an ancestral role for Mitf genes in promoting the development of melanophores and xanthophores, with partitioning of this role to varying degrees between paralogous Mitf genes in teleosts. As additional mutants are produced and discovered, it will be interesting to learn if cooperative functions of Mitf and Tfec genes represent a shared ancestral feature of pigmentary systems across ectotherms.

Author Contributions

Katia G. Korzeniwsky: investigation, visualization, formal analysis, writing – review and editing, validation. **Pietro L.H. de Mello:** formal analysis, writing – review and editing, visualization, methodology. **Yipeng Liang:** writing – review and editing, investigation. **McKenna Feltes:** resources. **Steven A. Farber:** resources. **David M. Parichy:** project administration, visualization, conceptualization, funding acquisition, writing – original draft, writing – review and editing, formal analysis, supervision, resources, validation.

Acknowledgements

Supported by NIH R35 GM122471 (D.M.P.), NIH R01 DK093399 (S.A.F.) and NIH F32 GM144223 (M.F.). Thanks to L.B. Patterson for assistance with imaging adult fish, A. Carr for assistance with super-resolution imaging of dying cells, and D. Huang for advice on imaging and other technical aspects of the work.

Conflicts of Interest

The authors declare no conflicts of interest.

Data Availability Statement

The data that support the findings of this study are available from the corresponding author upon reasonable request.

References

Aman, A. J., L. M. Saunders, A. A. Carr, et al. 2023. "Transcriptomic Profiling of Tissue Environments Critical for Post-Embryonic Patterning and Morphogenesis of Zebrafish Skin." *eLife* 12: 6670. https://doi.org/10.7554/eLife.86670.

Baranasic, D., M. Hortenhuber, P. J. Balwierz, et al. 2022. "Multiomic Atlas With Functional Stratification and Developmental Dynamics of Zebrafish Cis-Regulatory Elements." *Nature Genetics* 54, no. 7: 1037–1050. https://doi.org/10.1038/s41588-022-01089-w.

Bharti, K., M. Gasper, J. Ou, et al. 2012. "A Regulatory Loop Involving PAX6, MITF, and WNT Signaling Controls Retinal Pigment Epithelium Development." *PLoS Genetics* 8, no. 7: e1002757. https://doi.org/10.1371/journal.pgen.1002757.

Bowen, M. E., K. Henke, K. R. Siegfried, M. L. Warman, and M. P. Harris. 2012. "Efficient Mapping and Cloning of Mutations in Zebrafish

by Low-Coverage Whole-Genome Sequencing." *Genetics* 190, no. 3: 1017–1024. https://doi.org/10.1534/genetics.111.136069.

Brombin, A., and E. E. Patton. 2024. "Melanocyte Lineage Dynamics in Development, Growth and Disease." *Development* 151, no. 15: 1266. https://doi.org/10.1242/dev.201266.

Budi, E. H., L. B. Patterson, and D. M. Parichy. 2011. "Post-Embryonic Nerve-Associated Precursors to Adult Pigment Cells: Genetic Requirements and Dynamics of Morphogenesis and Differentiation." *PLoS Genetics* 7, no. 5: e1002044. https://doi.org/10.1371/journal.pgen.1002044.

Cao, J., M. Spielmann, X. Qiu, et al. 2019. "The Single-Cell Transcriptional Landscape of Mammalian Organogenesis." *Nature* 566, no. 7745: 496–502. https://doi.org/10.1038/s41586-019-0969-x.

Chen, S., Y. Zhou, Y. Chen, and J. Gu. 2018. "Fastp: An Ultra-Fast All-In-One FASTQ Preprocessor." *Bioinformatics* 34, no. 17: i884–i890. https://doi.org/10.1093/bioinformatics/bty560.

Curran, K., J. A. Lister, G. R. Kunkel, A. Prendergast, D. M. Parichy, and D. W. Raible. 2010. "Interplay Between Foxd3 and Mitf Regulates Cell Fate Plasticity in the Zebrafish Neural Crest." *Developmental Biology* 344: 107–118. https://doi.org/10.1016/j.ydbio.2010.04.023.

Curran, K., D. W. Raible, and J. A. Lister. 2009. "Foxd3 Controls Melanophore Specification in the Zebrafish Neural Crest by Regulation of Mitf." *Developmental Biology* 332, no. 2: 408–417. https://doi.org/10.1016/j.ydbio.2009.06.010.

Czech, L., J. P. Spence, and M. Exposito-Alonso. 2024. "Grenedalf: Population Genetic Statistics for the Next Generation of Pool Sequencing." *Bioinformatics* 40, no. 8: 508. https://doi.org/10.1093/bioinformatics/btae508.

Danecek, P., J. K. Bonfield, J. Liddle, et al. 2021. "Twelve Years of SAMtools and BCFtools." *GigaScience* 10, no. 2: 8. https://doi.org/10.1093/gigascience/giab008.

Dilshat, R., V. Fock, C. Kenny, et al. 2021. "MITF Reprograms the Extracellular Matrix and Focal Adhesion in Melanoma." *eLife* 10: 63093. https://doi.org/10.7554/eLife.63093.

Dorsky, R. I., D. W. Raible, and R. T. Moon. 2000. "Direct Regulation of Nacre, a Zebrafish MITF Homolog Required for Pigment Cell Formation, by the Wnt Pathway." *Genes & Development* 14, no. 2: 158–162.

El-Brolosy, M. A., Z. Kontarakis, A. Rossi, et al. 2019. "Genetic Compensation Triggered by Mutant mRNA Degradation." *Nature* 568, no. 7751: 193–197. https://doi.org/10.1038/s41586-019-1064-z.

Elworthy, S. 2003. "Transcriptional Regulation of Mitfa Accounts for the sox10 Requirement in Zebrafish Melanophore Development." *Development* 130, no. 12: 2809–2818. https://doi.org/10.1242/dev.00461.

Eom, D. S., S. Inoue, L. B. Patterson, et al. 2012. "Melanophore Migration and Survival During Zebrafish Adult Pigment Stripe Development Require the Immunoglobulin Superfamily Adhesion Molecule Igsf11." *PLoS Genetics* 8, no. 8: e1002899. https://doi.org/10.1371/journal.pgen.1002899.

Frohnhofer, H. G., J. Krauss, H. M. Maischein, and C. Nusslein-Volhard. 2013. "Iridophores and Their Interactions With Other Chromatophores Are Required for Stripe Formation in Zebrafish." *Development* 140, no. 14: 2997–3007. https://doi.org/10.1242/dev.096719.

Garcia- Elfring, A., C. E. Sabin, A. L. Iouchmanov, et al. 2023. "Piebaldism and Chromatophore Development in Reptiles Are Linked to the Tfec Gene." *Current Biology* 33, no. 4: 755–763. https://doi.org/10.1016/j.cub.2023.01.004.

Goding, C. R., and H. Arnheiter. 2019. "MITF-The First 25 Years." *Genes & Development* 33, no. 15–16: 983–1007. https://doi.org/10.1101/gad.324657.119.

Gur, D., E. J. Bain, K. R. Johnson, et al. 2020. "In Situ Differentiation of Iridophore Crystallotypes Underlies Zebrafish Stripe Patterning." *Nature Communications* 11, no. 1: 6391. https://doi.org/10.1038/s41467-020-20088-1.

Hallsson, J. H., J. Favor, C. Hodgkinson, et al. 2000. "Genomic, Transcriptional and Mutational Analysis of the Mouse Microphthalmia Locus." *Genetics* 155, no. 1: 291–300. https://doi.org/10.1093/genetics/155.1.291.

Hansdottir, A. G., K. Palsdottir, J. Favor, et al. 2004. "The Novel Mouse Microphthalmia Mutations Mitfmi-enu5 and Mitfmi-bcc2 Produce Dominant Negative Mitf Proteins." *Genomics* 83, no. 5: 932–935. https://doi.org/10.1016/j.ygeno.2003.10.013.

Hemesath, T. J., E. Steingrimsson, G. McGill, et al. 1994. "Microphthalmia, a Critical Factor in Melanocyte Development, Defines a Discrete Transcription Factor Family." *Genes & Development* 8, no. 22: 2770–2780. https://doi.org/10.1101/gad.8.22.2770.

Henke, K., J. M. Daane, M. B. Hawkins, et al. 2017. "Genetic Screen for Postembryonic Development in the Zebrafish (*Danio rerio*): Dominant Mutations Affecting Adult Form." *Genetics* 207, no. 2: 609–623. https://doi.org/10.1534/genetics.117.300187.

Hodgkinson, C. A., K. J. Moore, A. Nakayama, et al. 1993. "Mutations at the Mouse Microphthalmia Locus Are Associated With Defects in a Gene Encoding a Novel Basic-Helix-Loop-Helix-Zipper Protein." *Cell* 74, no. 2: 395–404.

Hodgkinson, C. A., A. Nakayama, H. Li, et al. 1998. "Mutation at the Anophthalmic White Locus in Syrian Hamsters: Haploinsufficiency in the Mitf Gene Mimics Human Waardenburg Syndrome Type 2." *Human Molecular Genetics* 7, no. 4: 703–708. https://doi.org/10.1093/hmg/7.4.703.

Hoshijima, K., M. J. Jurynec, D. Klatt Shaw, A. M. Jacobi, M. A. Behlke, and D. J. Grunwald. 2019. "Highly Efficient CRISPR-Cas9-Based Methods for Generating Deletion Mutations and F0 Embryos That Lack Gene Function in Zebrafish." *Developmental Cell* 51, no. 5: 645–657. https://doi.org/10.1016/j.devcel.2019.10.004.

Huang, D., E. H. Kapadia, Y. Liang, et al. 2025. "Agouti and BMP Signaling Drive a Naturally Occurring Fate Conversion of Melanophores to Leucophores in Zebrafish." *Proceedings of the National Academy of Sciences* 122, no. 8: e2424180122. https://doi.org/10.1073/pnas.2424180122.

Irion, U., A. P. Singh, and C. Nusslein-Volhard. 2016. "The Developmental Genetics of Vertebrate Color Pattern Formation: Lessons From Zebrafish." *Current Topics in Developmental Biology* 117: 141–169. https://doi.org/10.1016/bs.ctdb.2015.12.012.

Johnson, S. L., A. N. Nguyen, and J. A. Lister. 2011. "Mitfa Is Required at Multiple Stages of Melanocyte Differentiation but Not to Establish the Melanocyte Stem Cell." *Developmental Biology* 350, no. 2: 405–413. https://doi.org/10.1016/j.ydbio.2010.12.004.

Kelsh, R. N., K. Camargo Sosa, S. Farjami, V. Makeev, J. H. P. Dawes, and A. Rocco. 2021. "Cyclical Fate Restriction: A New View of Neural Crest Cell Fate Specification." *Development* 148, no. 22: 6057. https://doi.org/10.1242/dev.176057.

Kenny, C., R. Dilshat, H. E. Seberg, et al. 2022. "TFAP2 Paralogs Facilitate Chromatin Access for MITF at Pigmentation and Cell Proliferation Genes." *PLoS Genetics* 18, no. 5: e1010207. https://doi.org/10.1371/journal.pgen.1010207.

Kimmel, C. B., W. W. Ballard, S. R. Kimmel, B. Ullmann, and T. F. Schilling. 1995. "Stages of Embryonic Development of the Zebrafish." *Developmental Dynamics* 203, no. 3: 253–310.

Kontarakis, Z., and D. Y. R. Stainier. 2020. "Genetics in Light of Transcriptional Adaptation." *Trends in Genetics* 36, no. 12: 926–935. https://doi.org/10.1016/j.tig.2020.08.008.

Lane, B. M., and J. A. Lister. 2012. "Otx but Not Mitf Transcription Factors Are Required for Zebrafish Retinal Pigment Epithelium Development." *PLoS One* 7, no. 11: e49357. https://doi.org/10.1371/journal.pone.0049357.

Langmead, B., and S. L. Salzberg. 2012. "Fast Gapped-Read Alignment With Bowtie 2." *Nature Methods* 9, no. 4: 357–359. https://doi.org/10.1038/nmeth.1923.

Le Douarin, N. M. 1999. *The Neural Crest*. Cambride University Press.

Lewis, V. M., L. M. Saunders, T. A. Larson, et al. 2019. "Fate Plasticity and Reprogramming in Genetically Distinct Populations of Danio Leucophores." *Proceedings of the National Academy of Sciences of the United States of America* 116, no. 24: 11806–11811. https://doi.org/10.1073/pnas.1901021116.

Li, H. 2011. "A Statistical Framework for SNP Calling, Mutation Discovery, Association Mapping and Population Genetical Parameter Estimation From Sequencing Data." *Bioinformatics* 27, no. 21: 2987–2993. https://doi.org/10.1093/bioinformatics/btr509.

Lister, J. A., A. Capper, Z. Zeng, et al. 2014. "A Conditional Zebrafish MITF Mutation Reveals MITF Levels Are Critical for Melanoma Promotion vs. Regression In Vivo." *Journal of Investigative Dermatology* 134, no. 1: 133–140. https://doi.org/10.1038/jid.2013.293.

Lister, J. A., J. Close, and D. W. Raible. 2001. "Duplicate Mitf Genes in Zebrafish: Complementary Expression and Conservation of Melanogenic Potential." *Developmental Biology* 237, no. 2: 333–344.

Lister, J. A., B. M. Lane, A. Nguyen, and K. Lunney. 2011. "Embryonic Expression of Zebrafish MiT Family Genes Tfe3b, Tfeb, and Tfec." *Developmental Dynamics* 240, no. 11: 2529–2538. https://doi.org/10.1002/dvdy.22743.

Lister, J. A., C. P. Robertson, T. Lepage, S. L. Johnson, and D. W. Raible. 1999. "Nacre Encodes a Zebrafish Microphthalmia-Related Protein That Regulates Neural-Crest-Derived Pigment Cell Fate." *Development* 126, no. 17: 3757–3767.

Lopes, S. S., X. Yang, J. Muller, et al. 2008. "Leukocyte Tyrosine Kinase Functions in Pigment Cell Development." *PLoS Genetics* 4, no. 3: e1000026. https://doi.org/10.1371/journal.pgen.1000026.

Louphrasitthiphol, P., R. Siddaway, A. Loffreda, et al. 2020. "Tuning Transcription Factor Availability Through Acetylation-Mediated Genomic Redistribution." *Molecular Cell* 79, no. 3: 472–487. https://doi.org/10.1016/j.molcel.2020.05.025.

McLaren, W., L. Gil, S. E. Hunt, et al. 2016. "The Ensembl Variant Effect Predictor." *Genome Biology* 17, no. 1: 122. https://doi.org/10.1186/s13059-016-0974-4.

McMenamin, S. K., E. J. Bain, A. E. McCann, et al. 2014. "Thyroid Hormone-Dependent Adult Pigment Cell Lineage and Pattern in Zebrafish." *Science* 345, no. 6202: 1358–1361. https://doi.org/10.1126/science.1256251.

Minvielle, F., B. Bed'hom, J. L. Coville, S. Ito, M. Inoue-Murayama, and D. Gourichon. 2010. "The "Silver" Japanese Quail and the MITF Gene: Causal Mutation, Associated Traits and Homology With the "Blue" Chicken Plumage." *BMC Genetics* 11: 15. https://doi.org/10.1186/1471-2156-11-15.

Miyadai, M., H. Takada, A. Shiraishi, et al. 2023. "A Gene Regulatory Network Combining Pax3/7, Sox10 and Mitf Generates Diverse Pigment Cell Types in Medaka and Zebrafish." *Development* 150, no. 19: 2114. https://doi.org/10.1242/dev.202114.

Ng, P. C., and S. Henikoff. 2003. "SIFT: Predicting Amino Acid Changes That Affect Protein Function." *Nucleic Acids Research* 31, no. 13: 3812–3814. https://doi.org/10.1093/nar/gkg509.

Nonaka, M. c. 2012. *Remedios Varo: The Mexican Years*. Editorial RM.

Okonechnikov, K., A. Conesa, and F. Garcia-Alcalde. 2016. "Qualimap 2: Advanced Multi-Sample Quality Control for High-Throughput Sequencing Data." *Bioinformatics* 32, no. 2: 292–294. https://doi.org/10.1093/bioinformatics/btv566.

Parichy, D. M. 2021. "Evolution of Pigment Cells and Patterns: Recent Insights From Teleost Fishes." *Current Opinion in Genetics & Development* 69: 88–96. https://doi.org/10.1016/j.gde.2021.02.006.

Parichy, D. M., M. R. Elizondo, M. G. Mills, T. N. Gordon, and R. E. Engeszer. 2009. "Normal Table of Postembryonic Zebrafish Development: Staging by Externally Visible Anatomy of the Living Fish." *Developmental Dynamics* 238: 2975–3015.

Parichy, D. M., D. G. Ransom, B. Paw, L. I. Zon, and S. L. Johnson. 2000. "An Orthologue of the *Kit*-Related Gene *Fms* Is Required for Development of Neural Crest-Derived Xanthophores and a Subpopulation of Adult Melanocytes in the Zebrafish, *Danio Rerio*." *Development* 127, no. 14: 3031–3044.

Parichy, D. M., and J. M. Turner. 2003. "Temporal and Cellular Requirements for Fms Signaling During Zebrafish Adult Pigment Pattern Development." *Development* 130, no. 5: 817–833.

Patterson, L. B., and D. M. Parichy. 2013. "Interactions With Iridophores and the Tissue Environment Required for Patterning Melanophores and Xanthophores During Zebrafish Adult Pigment Stripe Formation." *PLoS Genetics* 9, no. 5: e1003561. https://doi.org/10.1371/journal.pgen.1003561.

Peri, F., and C. Nusslein-Volhard. 2008. "Live Imaging of Neuronal Degradation by Microglia Reveals a Role for v0-ATPase a1 in Phagosomal Fusion In Vivo." *Cell* 133, no. 5: 916–927. https://doi.org/10.1016/j.cell.2008.04.037.

Petratou, K., S. A. Spencer, R. N. Kelsh, and J. A. Lister. 2021. "The MITF Paralog Tfec Is Required in Neural Crest Development for Fate Specification of the Iridophore Lineage From a Multipotent Pigment Cell Progenitor." *PLoS One* 16, no. 1: e0244794. https://doi.org/10.1371/journal.pone.0244794.

Petratou, K., T. Subkhankulova, J. A. Lister, A. Rocco, H. Schwetlick, and R. N. Kelsh. 2018. "A Systems Biology Approach Uncovers the Core Gene Regulatory Network Governing Iridophore Fate Choice From the Neural Crest." *PLoS Genetics* 14, no. 10: e1007402. https://doi.org/10.1371/journal.pgen.1007402.

Philipp, U., B. Lupp, S. Momke, et al. 2011. "A MITF Mutation Associated With a Dominant White Phenotype and Bilateral Deafness in German Fleckvieh Cattle." *PLoS One* 6, no. 12: e28857. https://doi.org/10.1371/journal.pone.0028857.

Pogenberg, V., M. H. Ogmundsdottir, K. Bergsteinsdottir, et al. 2012. "Restricted Leucine Zipper Dimerization and Specificity of DNA Recognition of the Melanocyte Master Regulator MITF." *Genes & Development* 26, no. 23: 2647–2658. https://doi.org/10.1101/gad.198192.112.

Prendergast, A., T. H. Linbo, T. Swarts, et al. 2012. "The Metalloproteinase Inhibitor Reck Is Essential for Zebrafish DRG Development." *Development* 139, no. 6: 1141–1152. https://doi.org/10.1242/dev.072439.

Ran, R., L. Li, T. Xu, J. Huang, H. He, and Y. Chen. 2024. "Revealing Mitf Functions and Visualizing Allografted Tumor Metastasis in Colorless and Immunodeficient *Xenopus tropicalis*." *Communications Biology* 7, no. 1: 275. https://doi.org/10.1038/s42003-024-05967-3.

Saunders, L. M., A. J. Aman, A. K. Mishra, et al. 2019. "Thyroid Hormone Regulates Distinct Paths to Maturation in Pigment Cell Lineages." *eLife* 8: e45181.

Schartl, M., L. Larue, M. Goda, M. W. Bosenberg, H. Hashimoto, and R. N. Kelsh. 2016. "What Is a Vertebrate Pigment Cell?" *Pigment Cell & Melanoma Research* 29, no. 1: 8–14. https://doi.org/10.1111/pcmr.12409.

Sim, N. L., P. Kumar, J. Hu, S. Henikoff, G. Schneider, and P. C. Ng. 2012. "SIFT Web Server: Predicting Effects of Amino Acid Substitutions on Proteins." *Nucleic Acids Research* 40: W452–W457. https://doi.org/10.1093/nar/gks539.

Singh, A. P., A. Dinwiddie, P. Mahalwar, et al. 2016. "Pigment Cell Progenitors in Zebrafish Remain Multipotent Through Metamorphosis." *Developmental Cell* 38, no. 3: 316–330. https://doi.org/10.1016/j.devcel.2016.06.020.

Solnica-Krezel, L., A. F. Schier, and W. Driever. 1994. "Efficient Recovery of ENU-Induced Mutations From the Zebrafish Germline." *Genetics* 136, no. 4: 1401–1420.

Steingrimsson, E., K. J. Moore, M. L. Lamoreux, et al. 1994. "Molecular Basis of Mouse Microphthalmia (Mi) Mutations Helps Explain Their Developmental and Phenotypic Consequences." *Nature Genetics* 8, no. 3: 256–263. https://doi.org/10.1038/ng1194-256.

Sur, A., Y. Wang, P. Capar, G. Margolin, M. K. Prochaska, and J. A. Farrell. 2023. "Single-Cell Analysis of Shared Signatures and Transcriptional Diversity During Zebrafish Development." *Developmental Cell* 58, no. 24: 3028–3047. https://doi.org/10.1016/j.devcel.2023.11.001.

Tachibana, M. 1997. "Evidence to Suggest That Expression of MITF Induces Melanocyte Differentiation and Haploinsufficiency of MITF Causes Waardenburg Syndrome Type 2A." *Pigment Cell Research* 10, no. 1–2: 25–33. https://doi.org/10.1111/j.1600-0749.1997.tb00462.x.

Tadokoro, R., and Y. Takahashi. 2017. "Intercellular Transfer of Organelles During Body Pigmentation." *Current Opinion in Genetics & Development* 45: 132–138. https://doi.org/10.1016/j.gde.2017.05.001.

Tassabehji, M., V. E. Newton, and A. P. Read. 1994. "Waardenburg Syndrome Type 2 Caused by Mutations in the Human Microphthalmia (MITF) Gene." *Nature Genetics* 8, no. 3: 251–255. https://doi.org/10.1038/ng1194-251.

Taylor, K. L., J. A. Lister, Z. Zeng, et al. 2011. "Differentiated Melanocyte Cell Division Occurs In Vivo and Is Promoted by Mutations in Mitf." *Development* 138, no. 16: 3579–3589. https://doi.org/10.1242/dev.064014.

Team, R. C. 2021. *R: A Language and Environment for Statistical Computing*. R Foundation for Statistical Computing.

Tzika, A. C. 2024. "On the Role of TFEC in Reptilian Coloration." *Frontiers in Cell and Development Biology* 12: 1358828. https://doi.org/10.3389/fcell.2024.1358828.

Ullate-Agote, A., and A. C. Tzika. 2021. "Characterization of the Leucistic Texas Rat Snake *Pantherophis obsoletus*." *Frontiers in Ecology and Evolution* 9: 3136. https://doi.org/10.3389/fevo.2021.583136.

Vibert, L., G. Aquino, I. Gehring, et al. 2017. "An Ongoing Role for Wnt Signaling in Differentiating Melanocytes In Vivo." *Pigment Cell & Melanoma Research* 30, no. 2: 219–232. https://doi.org/10.1111/pcmr.12568.

Vu, H. N., R. Dilshat, V. Fock, and E. Steingrimsson. 2021. "User Guide to MiT-TFE Isoforms and Post-Translational Modifications." *Pigment Cell & Melanoma Research* 34, no. 1: 13–27. https://doi.org/10.1111/pcmr.12922.

Wang, C., B. Lu, T. Li, et al. 2021. "Nile Tilapia: A Model for Studying Teleost Color Patterns." *Journal of Heredity* 112, no. 5: 469–484. https://doi.org/10.1093/jhered/esab018.

Yamamoto, K., K. Okamura, K. Wakamatsu, et al. 2024. "Genetic Insights Into Tietz Albinism-Deafness Syndrome: A New Dominant-Negative Mutation in MITF." *Pigment Cell & Melanoma Research* 37, no. 4: 430–437. https://doi.org/10.1111/pcmr.13166.

Zeng, Z., S. L. Johnson, J. A. Lister, and E. E. Patton. 2015. "Temperature-Sensitive Splicing of Mitfa by an Intron Mutation in Zebrafish." *Pigment Cell & Melanoma Research* 28, no. 2: 229–232. https://doi.org/10.1111/pcmr.12336.

Zhou, Z., M. Li, H. Cheng, et al. 2018. "An Intercross Population Study Reveals Genes Associated With Body Size and Plumage Color in Ducks." *Nature Communications* 9, no. 1: 2648. https://doi.org/10.1038/s41467-018-04868-4.

Supporting Information

Additional supporting information can be found online in the Supporting Information section.

Dominant negative Mitf allele impacts melanophore and xanthophore development and reveals collaborative interactions with Tfec in zebrafish chromatophore lineages

Katia G. Korzeniwsky[1] | Pietro H. de Mello[1] | Yipeng Liang[1] | McKenna Feltes[2] | Steven A. Farber[2] | David M. Parichy[1,3]

[1] Department of Biology, University of Virginia, Charlottesville, Virginia, USA
[2] Department of Biology, Johns Hopkins University, Baltimore, Maryland, USA
[3] Department of Cell Biology, University of Virginia, Charlottesville, Virginia, USA

Supplementary Figures S1–S8

Supplementary Movies 1–5 legends

Supplementary references

FIGURE S1 | Post-embryonic pigment cells of body and fins. (a) Numbers of melanophores and xanthophores were similar between wild-type and *varo*/+ sibling adults (Wilcoxon: mel, S=32, *P*=0.4; xan, S=29, *P*=0.8; *n*=5 individuals of each genotype). (b) Melanin contents of cells were reduced in *varo*/+ relative to wild-type, as estimated by areas of aggregated melanosomes following epinephrine treatment (Huang et al., 2025; McCluskey et al., 2021) (nested ANOVA, genotype effect: $F_{1,8}$=39.4, *P*=0.0002; individuals treated as random effect within genotype; n=5 individuals of each genotype, 2465 total melanophores; original data collected with arbitrary units of pixels^2 and *ln*-transformed for analysis to correct for increased residual variance with larger predicted values). (c) Corresponding images illustrate xanthophore carotenoid accumulations post-epinephrine treatment in full color and pseudocolor; details of the same *varo*/+ image as shown in Figure 1b. (d) Pigment cells of adult dorsal fin showing that melanoleucophores at the fin edge of wild-type (arrowheads) were mostly missing in *varo* heterozygotes whereas melanophores, xanthophores and melanoleucophores were entirely missing in *varo* homozygotes. In the anal fin, iridescent iridophores of fin rays and interstripes (arrows) in the wild type were present in *varo*/+ but were markedly fewer in *varo*-/-. Melanoleucophores and xantholeucophores and their genetic requirements have been described only recently (Huang et al., 2025; Lewis et al., 2019). Scale bars: c, 50 μm; d, 200 μm.

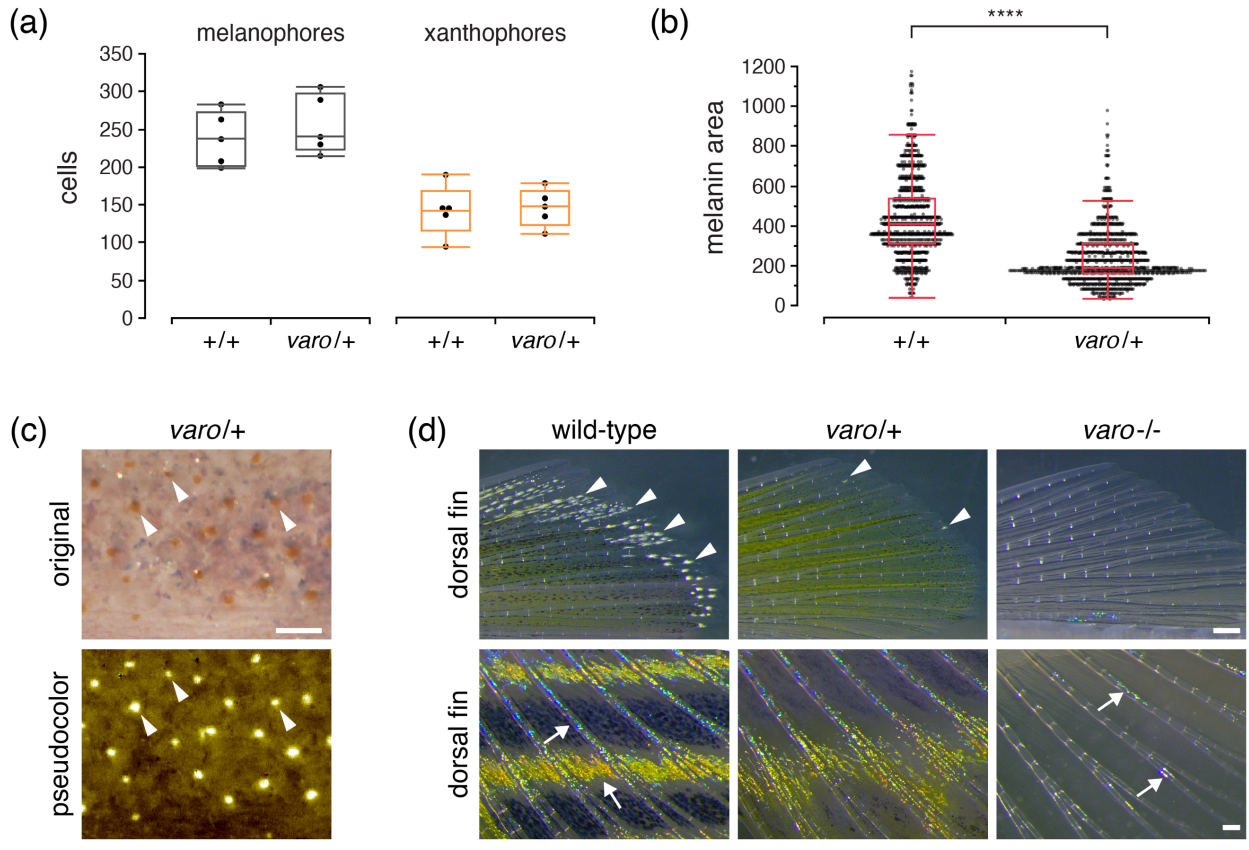

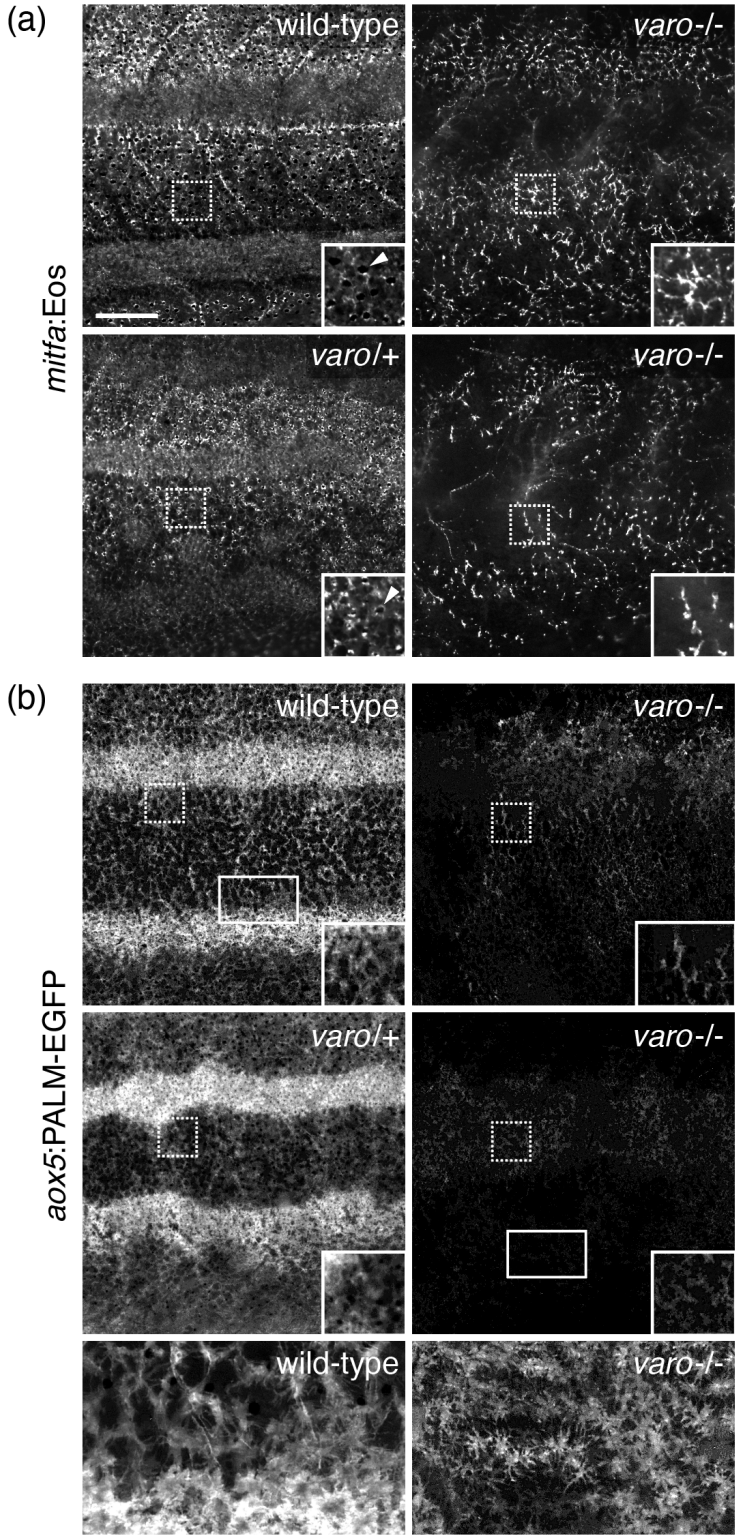

FIGURE S2 | Reporter expression in adults. Shown are regions of the trunk from wild-type and heterozygous *varo* mutants, as well as two examples from homozygous *varo* mutants. (a) *varo* mutant homozygotes developed variable numbers of *mitfa*+ cells. Many *mitfa*+ cells in wild-type and *varo*/+ were melanized (e.g., arrowheads in insets), whereas none of the *mitfa*+ cells of *varo*-/- had discernible melanin. All images acquired at same exposure. (b) In contrast to embryonic and early larval stages, *varo*-/- mutants developed numerous unpigmented *aox5*+ cells, most of which expressed only low levels of reporter. All images acquired at same settings and displayed with same settings in upper four panels and insets. Bottom two panels show regions of solid rectangles in wild-type and lower right *varo*-/- mutant at higher display values, revealing low-expressing *aox5*+ cells in the mutant with highly dendritic morphologies not typical of pigmented xanthophores in light interstripes or cryptic unpigmented xanthophores in stripes (McMenamin et al., 2014; Saunders et al., 2019). Scale bar: in a, for a and b, 500 μm.

FIGURE S3 | Mutant alleles induced in MiT subfamily genes. (a) CRISPR/Cas9 alleles detected in homozygous or compound heterozygous individuals used for analyses. Red nucleotides are novel, dashes indicate deletions relative to wild-type. Numbers at right indicate total frame-shifts by insertion, deletion, or both. All alleles led to premature termination codons and differences in phenotype were not apparent in for alleles or combinations of alleles within loci. (b) Reverse transcriptase PCR of cDNAs from 24 hpf embryos of wild-type, *mitfa*^{del}, *mitfa*^{w2}, and *mitfa*^{varo} individuals, with no-template control, illustrating absence of *mitfa* transcript in *mitfa*$^{del/del}$ individuals, with primers to amplify full length or an internal region of cDNA.

(a)

AltR262

mitfa	5′-GACAAAGCTGGACCATGTGGCAAGTTTGACTCTTATCAAAGACCT-3′	
mitfa—vp70rc1varo	5′-GACAAAGCTGGACCATGT-------TTGACTCTTATCAAAGACCT-3′	(-7)

AltR471

mitfb	5′-TGCCTCCTCCA.....GGAATCTCCATCAGTAACTCCTGTCCTGC-3′	
mitfb—vp75rc1	5′-TGCCTCCTCCAaactcgttcatgttaaCAGTAACTCCTGTCCTGC-3′	(+16)
mitfb—vp75rc2	5′-TGCCTC----------TCCATCAGTAACTCCTGTCCTGC-3′	(-16)
mitfb—vp75rc3	5′-T--------CA.....GGAATCTCCATCAGTAACTCCTGTCCTGC-3′	(-8)
mitfb—vp75rc4	5′-TGCCTCa----------CCATCAGTAACTCCTGTCCTGC-3′	(-16)
mitfb—vp75rc5	5′-TGCCTC----------TCCATCAGTAACTCCTGTCCTGC-3′	(-16)

AltR466

tfec	5′-TCAGTTTCCGATGGA....TGAAGTTATTGACGATCTTATTGGCC-3′	
tfec—vp76rc1	5′-TCAGTTTCCGATG--....--AAGTTATTGACGATCTTATTGGCC-3′	(-4)
tfec—vp76rc2	5′-TCAGTTTCCGATGaAgacagaAAGTTATTGACGATCTTATTGGCC-3′	(+4)
tfec—vp76rc3	5′-TCAGTTTCCGA----....---AGTTATTGACGATCTTATTGGCC-3′	(-7)

(b)

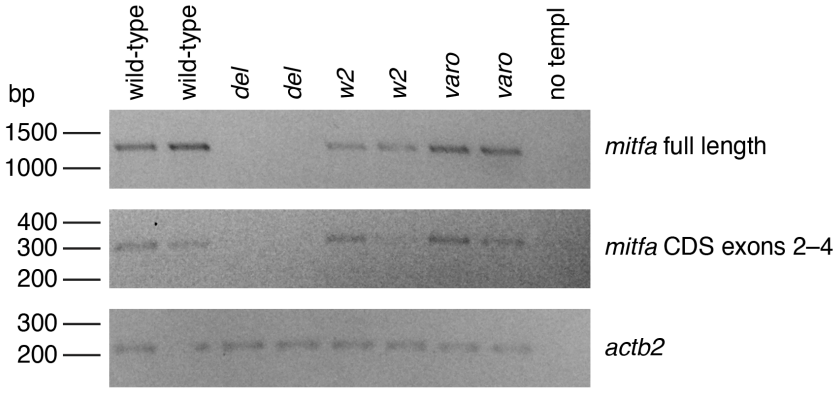

FIGURE S4 | Death of *mitfa*:Eos+ cells in *varo* mutants during stages of embryonic pigment cell development. Embryos for these analyses were reared to 35 hpf then imaged at super-resolution, without collecting time-lapse movies. (a) Normal morphologies of *mitfa*:Eos+ cells in wild-type embryos near the dorsal myotome (dotted line, upper panels) and further ventrally (lower panels; *, position of lateral line. Arrowheads in left panels indicate cells shown at higher magnification in right panels. Arrow, one of many filopodia often present on healthy cells, Granular appearance of cells may be indicative of developing melanosomes. (b) Examples of *mitfa*:Eos+ cellular debris (upper, arrowhead) as well as anomalous blebbed morphology of *mitfa*:Eos+ cell (lower, arrowhead) and additional cellular debris (some highlighted with brackets). Scale bars: in b, for a and b, 20 μm (left panels) and 10 μm (right panels).

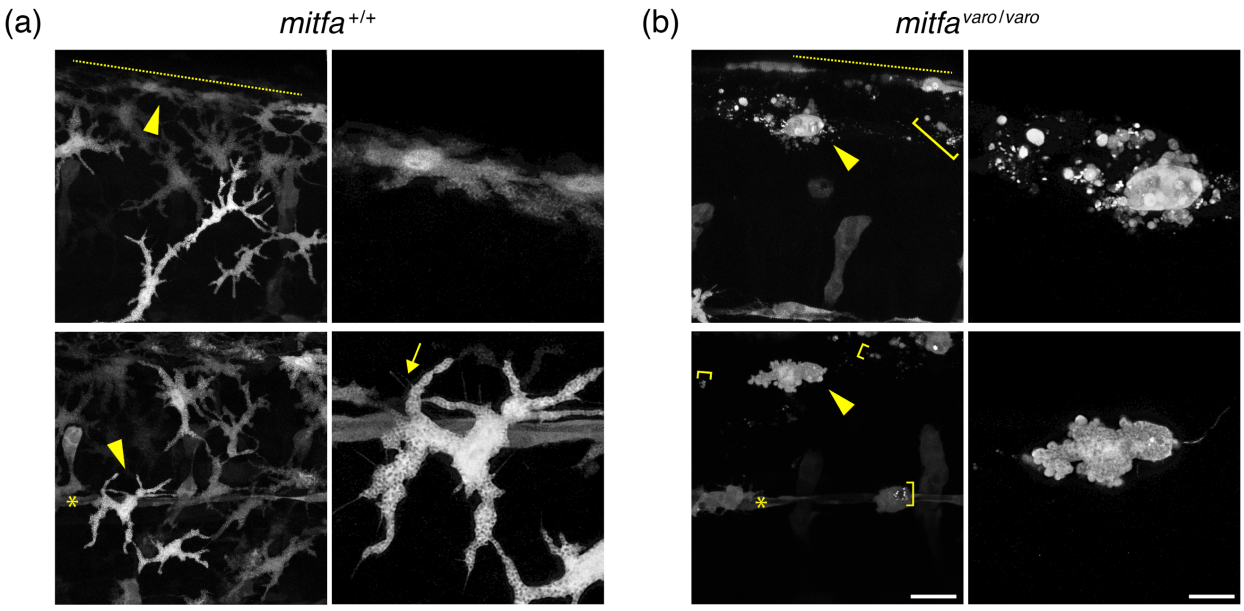

FIGURE S5 | Iridophore phenotypes of early larvae. (a) Dorsal iridophores at 4 days post-fertilization, with each point representing the iridophore complement of a single larva. Whereas *mitfa*^{varo} heterozygotes and homozygotes had counts not significantly different from wild-type (same observation referred to in the legend of Figure 1), larvae homozygous for *mitfa*^{w2} or *mitfa*^{del} had excess dorsal iridophores. Shared letters above groups indicate means not significantly different from one another in *post hoc* Tukey Kramer comparisons (overall ANOVA: $F_{4,72}$=80.1, P<0.0001). Diamond center lines indicate group means; diamond maxima and minima indicate 95% confidence limits. (b) Trunks and tails of representative early larvae showing different complements of iridescent iridophores across genotypes.

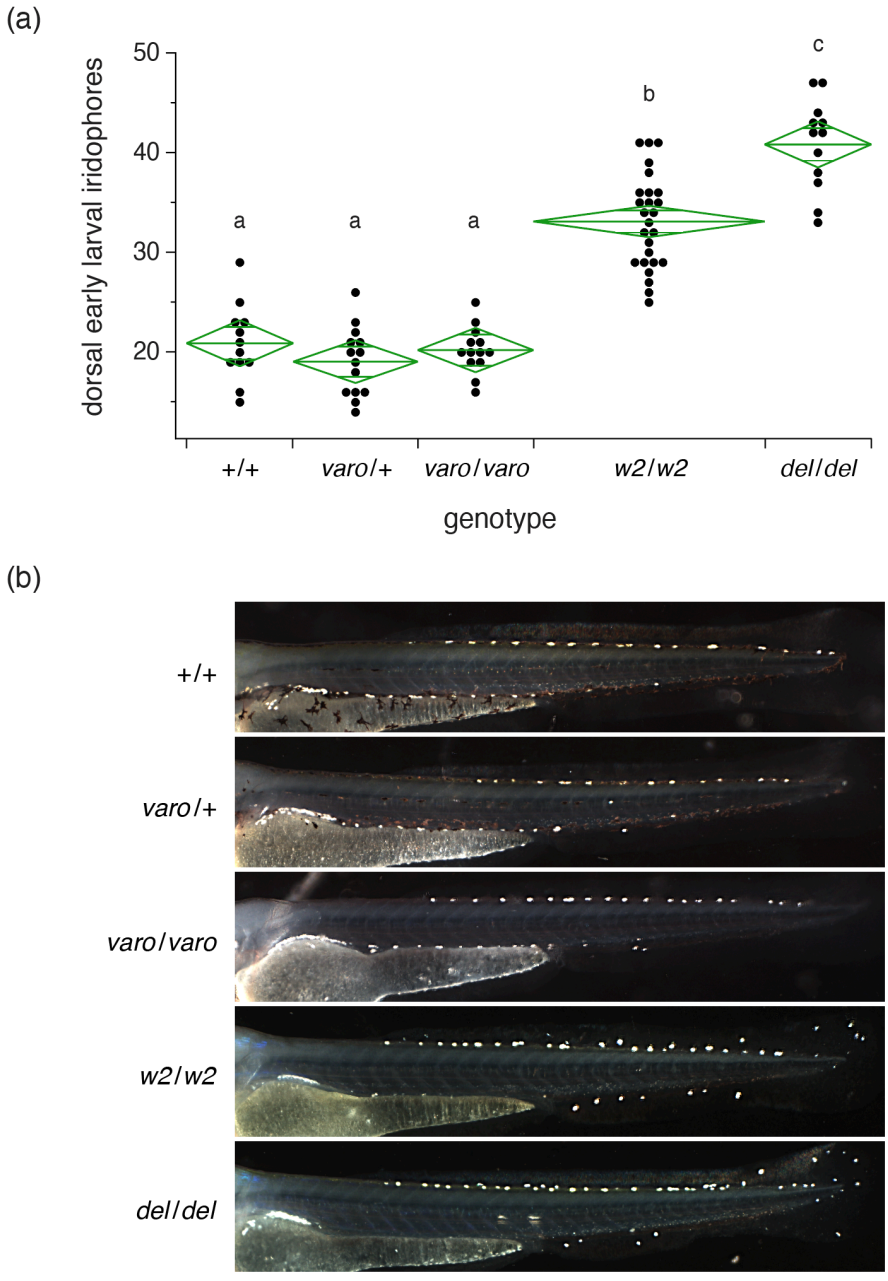

FIGURE S6 | Xanthophore pigmentation defect in *mitfa*^{vc7}. Homozygotes mutant for the temperature-sensitive allele had reduced yellow coloration at temperatures that were both intermediate (27°C) and restrictive (32°C) for the temperature-sensitive splicing defect. These defects were more severe than those of premature termination alleles (e.g., Figure 5a). Wild-type and mutant siblings are shown.

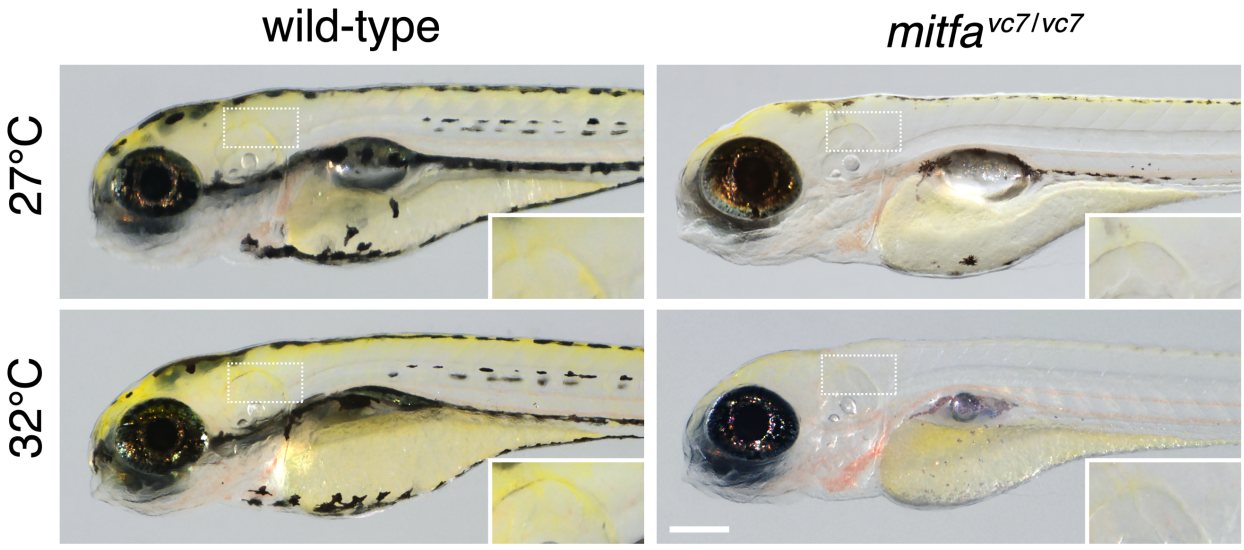

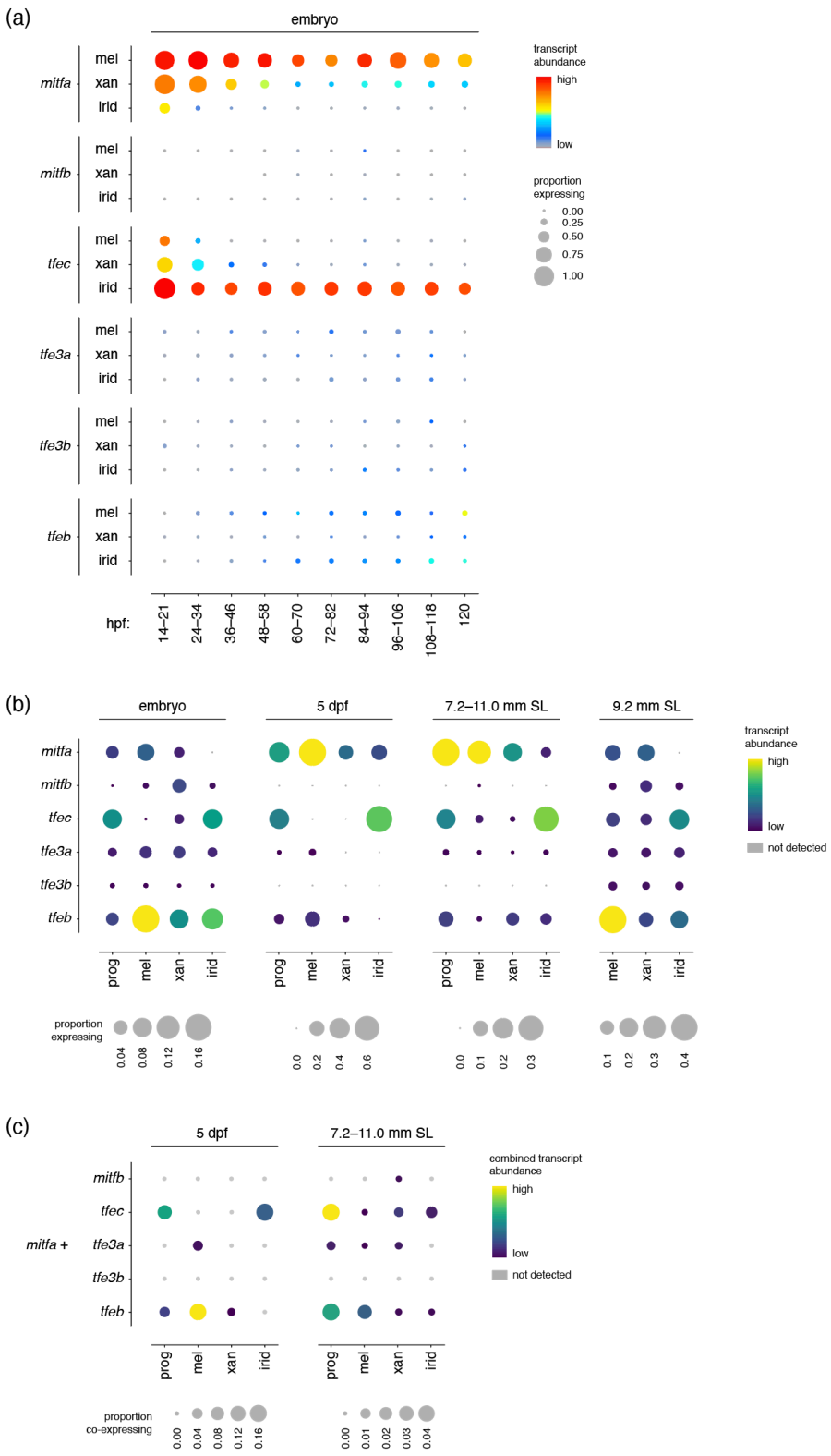

FIGURE S7 | Expression of *mitfa* and other MiT subfamily bHLH-ZIP transcription factor genes in published single cell transcriptomic datasets. Dot plots indicate transcript abundance and proportions of cells expressing *mitfa* and each of five MiT subfamily transcription factor genes. (a) Data for embryos at different hours post-fertilization (hpf) from daniocell.nichd.nih.gov (Sur et al., 2023). (b) Data from embryos (Saunders et al., 2023), 5 day post-fertilization (dpf) larvae and 7.2–11.0 mm standard length (SL) larvae (Saunders et al., 2019), and 9.2 mm SL larval skin (Aman et al., 2023). Note that published data sets for embryos in a and b are consistent with one another for some loci (e.g., *mitfa* and *tfec*) and at variance with one another for other loci (e.g., *mitfb*, *tfeb*). (c) Combined transcript abundances for cells identified to co-express *mitfa* with at least one other related transcription factor gene in single cell RNA-sequencing of Saunders et al. (2019) and Aman et al. (2023). Combined abundance of *mitfa* and *tfec* were particularly high for pigment cell progenitors.

FIGURE S8 | Double and single mutant phenotypes for *mitfa* and related genes and induced mutations. (a) Whole-fish phenotypes illustrating: phenotypic differences between *mitfa*^{w2} and *mitfb*, and reduced xanthophore pigmentation in fins of *mitfa*^{w2}*; mitfb* double mutant; near-absence of iridophores, reduced melanophores and persisting xanthophore pigmentation in *tfec* mutant (arrowhead, residual interstripe iridophores); loss of all pigment cells in *mitfa*^{w2}*; tfec* double mutant; irregular and hypopigmented pattern of *mitfa*$^{varo/+}$ and absence of melanophores and xanthophores in *mitfa*$^{varo/varo}$. (b) Late-stage larvae (~9.5 mm SL) heterozygous or homozygous for *tfec* mutation, illustrating persisting xanthophores (arrowheads and insets) and differences in overall pattern associated with loss of iridophores in homozygous mutant. (Fish not treated with epinephrine.) (c) Early larvae at 3 dpf and 4 dpf illustrate delayed xanthophore differentiation in *tfec* mutants and lack of xanthophores in *mitfa*^{w2}*; tfec* double mutants.

Figure appears on next page.

FIGURE S8 | Single and double mutant phenotypes for *mitfa* and related genes and induced mutations.

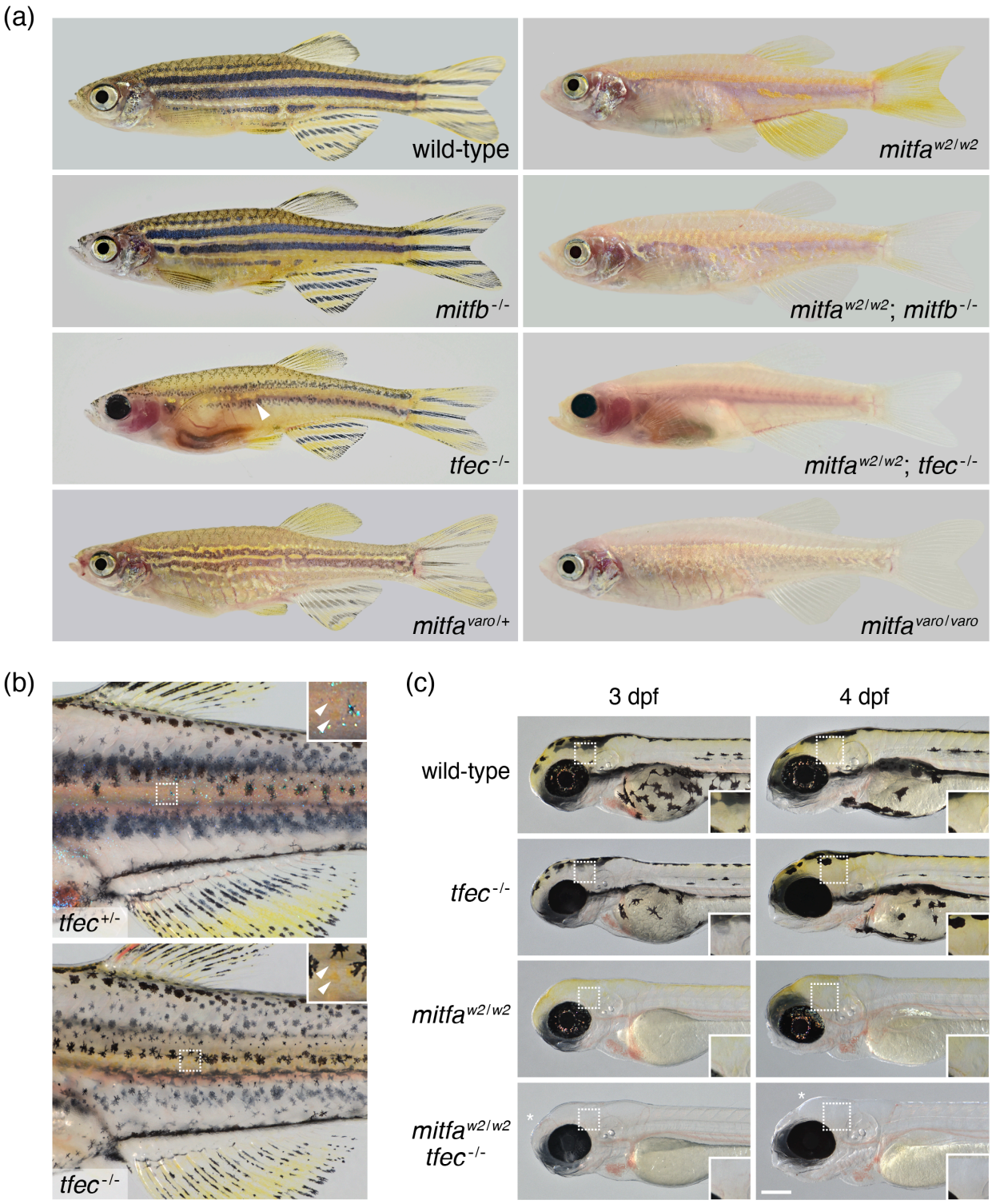

MOVIE 1 | Time-lapse imaging of wild-type *mitfa*:Eos+ cells over yolk extension, beginning at 22 hpf. Total time, 20 h; interval, 10 min 45 sec. Sibling embryos shown in Movies 2 and 3. Notochord and neural tube are faintly visible in medial portions of the embryo (see Figure 4a).

MOVIE 2 | Time-lapse imaging of *mitfa*^{varo}-/- *mitfa*:Eos+ cells; parameters as in Movie 1. Cells traveling from anterior (left) to posterior (right) beginning about half way into the movie are *mitfa*+ cells associated with the migrating lateral line primordium (present also, but more subtly, in Movie 1); whether these *mitfa*+ cells resemble other *mitfa*+ cells or lateral line associated glia is not known.

MOVIE 3 | Time-lapse imaging of *mitfa*^{varo}/+ *mitfa*:Eos+ cells; parameters as in Movie 1.

MOVIE 4 | Time-lapse imaging of *mitfa*^{w2}/+ *mitfa*:Eos+ cells over yolk extension, beginning at 22 hpf. Total time, 20 h; frame interval, 15 min.

MOVIE 5 | Time-lapse imaging of *mitfa*^{w2}-/- *mitfa*:Eos+ cells; parameters as in Movie 4.

SUPPLEMENTARY REFERENCES

Aman, A. J., Saunders, L. M., Carr, A. A., Srivatasan, S., Eberhard, C., Carrington, B., Watkins-Chow, D., Pavan, W. J., Trapnell, C., & Parichy, D. M. (2023). Transcriptomic profiling of tissue environments critical for post-embryonic patterning and morphogenesis of zebrafish skin. *Elife, 12*. doi:10.7554/eLife.86670

Huang, D., Kapadia, E. H., Liang, Y., Shriver, L. P., Dai, S., Patti, G. J., Humbel, B. M., Laudet, V., & Parichy, D. M. (2025). Agouti and BMP signaling drive a naturally occurring fate conversion of melanophores to leucophores in zebrafish. *Proceedings of the National Academy of Sciences, 122*(8), e2424180122. doi:10.1073/pnas.2424180122

Lewis, V. M., Saunders, L. M., Larson, T. A., Bain, E. J., Sturiale, S. L., Gur, D., Chowdhury, S., Flynn, J. D., Allen, M. C., Deheyn, D. D., Lee, J. C., Simon, J. A., Lippincott-Schwartz, J., Raible, D. W., & Parichy, D. M. (2019). Fate plasticity and reprogramming in genetically distinct populations of Danio leucophores. *Proc Natl Acad Sci U S A, 116*(24), 11806-11811. doi:10.1073/pnas.1901021116

McCluskey, B. M., Uji, S., Mancusi, J. L., Postlethwait, J. H., & Parichy, D. M. (2021). A complex genetic architecture in zebrafish relatives Danio quagga and D. kyathit underlies development of stripes and spots. *PLoS Genet, 17*(4), e1009364. doi:10.1371/journal.pgen.1009364

McMenamin, S. K., Bain, E. J., McCann, A. E., Patterson, L. B., Eom, D. S., Waller, Z. P., Hamill, J. C., Kuhlman, J. A., Eisen, J. S., & Parichy, D. M. (2014). Thyroid hormone-dependent adult pigment cell lineage and pattern in zebrafish. *Science, 345*(6202), 1358-1361. doi:10.1126/science.1256251

Saunders, L. M., Aman, A. J., Mishra, A. K., Lewis, V. M., Toomey, M. B., Packer, J. S., Qiu, X., McFaline-Figueroa, J. L., Corbo, J. C., Trapnell, C., & Parichy, D. M. (2019). Thyroid hormone regulates distinct paths to maturation in pigment cell lineages. *Elife, 8*, e45181.

Saunders, L. M., Srivatsan, S. R., Duran, M., Dorrity, M. W., Ewing, B., Linbo, T. H., Shendure, J., Raible, D. W., Moens, C. B., Kimelman, D., & Trapnell, C. (2023). Embryo-scale reverse genetics at single-cell resolution. *Nature*. doi:10.1038/s41586-023-06720-2

Sur, A., Wang, Y., Capar, P., Margolin, G., Prochaska, M. K., & Farrell, J. A. (2023). Single-cell analysis of shared signatures and transcriptional diversity during zebrafish development. *Dev Cell, 58*(24), 3028-3047 e3012. doi:10.1016/j.devcel.2023.11.001